

8-1-2018

Investigations into the Airside Cooling of a Heat Exchanger

David Vallet
davidvallet@gmail.com

Follow this and additional works at: <https://digitalscholarship.unlv.edu/thesesdissertations>

 Part of the [Mechanical Engineering Commons](#)

Repository Citation

Vallet, David, "Investigations into the Airside Cooling of a Heat Exchanger" (2018). *UNLV Theses, Dissertations, Professional Papers, and Capstones*. 3391.
<https://digitalscholarship.unlv.edu/thesesdissertations/3391>

This Thesis is protected by copyright and/or related rights. It has been brought to you by Digital Scholarship@UNLV with permission from the rights-holder(s). You are free to use this Thesis in any way that is permitted by the copyright and related rights legislation that applies to your use. For other uses you need to obtain permission from the rights-holder(s) directly, unless additional rights are indicated by a Creative Commons license in the record and/or on the work itself.

This Thesis has been accepted for inclusion in UNLV Theses, Dissertations, Professional Papers, and Capstones by an authorized administrator of Digital Scholarship@UNLV. For more information, please contact digitalscholarship@unlv.edu.

INVESTIGATIONS INTO THE AIRSIDE COOLING OF A HEAT EXCHANGER

By

David Vallet

Bachelor of Science – Applied Mathematics & Mathematics
University of South Africa
2014

Bachelor of Science Honours – Applied Mathematics
University of South Africa
2016

A thesis submitted in partial fulfillment
of the requirements for the

Master of Science in Engineering– Mechanical Engineering

Department of Mechanical Engineering
College of Engineering
The Graduate College

University of Nevada, Las Vegas
August 2018



Thesis Approval

The Graduate College
The University of Nevada, Las Vegas

June 29, 2018

This thesis prepared by

David Vallet

entitled

Investigations into the Airside Cooling of a Heat Exchanger

is approved in partial fulfillment of the requirements for the degree of

Master of Science in Engineering– Mechanical Engineering
Department of Mechanical Engineering

Samir Moujaes, Ph.D.
Examination Committee Chair

Kathryn Hausbeck Korgan, Ph.D.
Graduate College Interim Dean

William Culbreth, Ph.D.
Examination Committee Member

Mohamed Trabia, Ph.D.
Examination Committee Member

Stephen Lepp, Ph.D.
Graduate College Faculty Representative

ABSTRACT

In this study we investigate the air-side cooling of a flat-plate fin and tube heat transfer condenser with numerical simulations. A new design is proposed which utilises vortex generators to direct the flow in such a way as to remove some of the stagnant heated air that collects in the wake of the pipes. A comparative study of the proposed design and a standard tube and fin condenser is conducted by varying the air side entrance velocities. The Shear Stress Tension, SST $k - \omega$ 2-equation turbulent model is used to solve the RANS model in ANSYS Fluent 18. The results show an improved heat transfer gain with the proposed model at the expense of a greater pressure drop. We explain various analysis of the results concluding that the gains in heat transfer at higher air side face velocities are greater than the expense of power and that the proposed model is predicted to yield a flat-plate fin and pipe condenser that is more compact and energy efficient than the standard design. We predict the improvement of ideal power consumption over typical operating conditions on our portion of the condenser to be between 7% and 15%.

TABLE OF CONTENTS

ABSTRACT	iii
LIST OF FIGURES	vi
CHAPTER 1. INTRODUCTION	1
CHAPTER 2. FLUID DYNAMICS	4
Laminar Flow	4
Turbulent Flow	5
Flow around a cylinder	5
Flow through a channel	6
Hydrostatic diameter	6
Reynolds number	7
Fully Developed Flow	8
CHAPTER 3. HEAT TRANSFER	10
Conduction	10
Convection	11
Dimensionless numbers	12
Radiation	13
CHAPTER 4. MATHEMATICAL FORMULATION	14
Conservation of Mass	14
Conservation of Momentum	15
Conservation of Energy	16
Reynolds Averaged Navier Stokes Equations (RANS)	16
$\kappa - \omega$, <i>SST</i> equations.	18
CHAPTER 5. CFD SIMULATION	21
Finite Volume Method	21
Geometry	21
Classical Model	22
Proposed Model	23
Mesh	24
Convergence	27
Set-Up	31

CHAPTER 6. ANALYSIS	33
Convective Influence	33
Conductive Influence	41
Qualitative Analysis	42
Criticism of Design	51
Interpretation	52
CHAPTER 7. CONCLUSIONS	54
Future research	54
BIBLIOGRAPHY	55
CURRICULUM VITAE	57

LIST OF FIGURES

1	Left: a photograph of the chiller used in the experimental paper by Lee et al. Right: the dimensions of the chiller used in Lee et al. [22]	22
2	A close up view of the classic model, with flow lines	23
3	A close up view of the proposed model, with flow lines	24
4	A partial view of the mesh	26
5	Balance of heat flux over all surfaces Left: velocity 2.5 m/s Right: velocity 3.0 m/s	28
6	grid independence profile lines	28
7	grid independence plots of velocity along the length of our geometry.	29
8	grid independence plots of the temperature along the length of our geometry.	30
9	grid independence plots of temperature and velocity along the width of our geometry. Top: Velocity profile. Bottom: Temperature profile.	31
10	Top: Graphic showing the line along which the profiles are taken with an entrance velocity of 3m/s. Middle: Temperature profiles of classic and proposed model along line Bottom : Velocity profiles of classic and proposed model along line.	34
11	Top: Graphic showing the line along which the profiles are taken with an entrance velocity of 3m/s. Left: Temperature profiles of classic and proposed model along line. Right: Velocity profiles of classic and proposed model along line.	36
12	Mid-plane velocity contours with entrance velocities Top Left: 3.0m/s. Top Right: 3.5m/s. Bottom Left: 4.0m/s. Bottom Right: 5.0 m/s.	38
13	Mid-plane temperature contours with entrance velocities Top Left: 3.0 m/s. Top Right: 3.5 m/s. Bottom Left: 4.0 m/s. Bottom Right: 5.0 m/s.	40
14	Conduction through pipe and fins.	41
15	j-factor to Reynolds number	43
16	j-factor to Reynolds number	44
17	Volume Goodness (Kays and London 1984)	46
18	Volume Goodness (Bhowmik and Lee 2008)	47
19	thermohydraulic performance factor	48
20	Number of Thermal Units to Power Plot.	49
21	The heat flux as a function of Reynolds number	50
22	The heat flux as a function of Power	51
23	Chart of percentage gains and losses	52

CHAPTER 1

INTRODUCTION

Heat exchangers have been used throughout the world for millennia and today they are heavily relied upon by industries such as automotive, air conditioning and power plants. Designs of heat transfer devices today focus their attention on the size, weight, cost, and power consumption of the heat exchanger. Another consideration is the increasing scarcity of water as an evaporative agent which has led to forced convection becoming a more sought after and necessary mechanism for cooling. The improvement in the transfer of heat is often referred to as the heat augmentation and the main purpose of improving the augmentation is to make the heat exchangers either more compact or more efficient by reducing the pumping power. These feats are achieved through two classes of techniques, active and passive. Active techniques such as the use of electromagnetic waves or vibration, require the use of an additional external power source, while passive techniques require no direct application of added external power sources. Passive techniques revolve around altering the heat exchanger geometry, adding nano particles to the transfer fluids or the use of materials with improved conductive properties. Passive techniques can and may result in the use of more power to operate [21]. The subject of our investigation is the use of a passive technique by adding vortex generators to the geometry which disrupt the air-side flow of a flat-plate fin and tube heat exchanger to improve the augmentation.

There has been previous experimental work done on flat-plate fin and pipe heat exchangers,

notably various geometries and their surfaces were compared by Kays and London in 1984 [12], and later by Soland [19]. Both of these sought an approach to evaluating the compactness and efficiency of the condensers with Kays and London composing the 'area goodness' and 'volume goodness' factors. The 'area goodness' factor sought to define a graph for comparing the compactness of heat exchangers while the 'volume goodness' factor sought to define a convective comparison, we explain both of these in more detail later. The 'goodness factors' have since been modified slightly by Soland, et al [19] for their analysis. Comparative evaluations of designs with plate, wavy and louvered fins in fin-tube heat exchangers was conducted by Yan and Sheen in 1999 [25], who discovered that wavy fins had the highest 'area goodness' values, and louvered fins had the highest 'volume goodness' factors. A study of flat-plate fin condensers of varying tube rows, fin pitch and pipe diameter was done by Wang and Chi in 1999 [5], who found the heat transfer coefficient increased with a smaller fin pitch and the number of tube rows affected the heat transfer performance at low Reynolds numbers. Another study by Wang in 2002 [23] concerned enlarged designs of plate-fin condensers with either delta winglet or annular vortex generators placed around the pipe. In each of their designs they had 4 generators placed at equal radii around the pipe and forming a ring. Experiments by Wang et al [23] used water as the cooling convective fluid and sought to determine the streamline and friction effects of the varied vortex generator designs. The concluded that an increased pressure drop was found in all of his design, noting the penalty for the delta wing design was lower than the annular design. More recently with the advancement of computational power and numerical methods, CFD research has been conducted by Song, et al. 2010 [20] who created a double inclined rib design to disrupt the air-side flow. Tala, et al 2012 [18] distorted the pipe (tube) pattern by creating a more oval shape which led to improved flow around the pipe. Hwang et al, in 2012 [9] studied delta-wing vortex generators from frontal velocities of

0.5-20 m/s and found improvement in ‘area goodness’ for Reynolds numbers greater than 500. In a similar study to ours Singh and Sorensen presented a conference paper [17] in 2015 where a CFD study of vortex generators that are punched out of a split flat-plate fin and rise half the height of the flow channel, showed a marked improvement in the heat transfer with a vortex generator angled at 10° to the flow and a more recent experimental study by Wang, et al. [24] tested semi-dimple vortex generators against both flat-plate and louvered fin designs. They found that the louvered fins performed 2-15% better than the semi-dimple vortex generators which outperformed the flat-plate fin models.

In our study we focus on a design such that the condenser can be easily manufactured or converted to improve the heat transfer and save on energy costs. Our design inserts a fin style vortex generator perpendicular to and through each and every fin, parallel to the piping at 10° to the flow. In chapter 3 we describe the fluid dynamics of the airside of the condenser, as we seek to improve the augmentation of the condenser by altering the flow of air through the channel of the condenser a background knowledge of the main points involving the fluid dynamics concerned is explained. In chapter 4 we explain the relevant heat transfer mechanisms involved in our study. The mathematical formulation of our problem is explained in chapter 5 and an explanation of the computational fluid dynamic simulations that we ran are described in chapter 6 with an analysis of the results given in chapter 7. We then arrive at our conclusions in chapter 8.

CHAPTER 2

FLUID DYNAMICS

The subject of fluid flow has been the focus of research for generations and is very much on going. The flow of a liquid or gas is usually classified into one of three categories, laminar flow, turbulent flow or mixed flow. The properties of these flows can significantly alter the augmentation and convection. It is thus essential to determine the nature of the flow if one is to analyse an augmentation problem. The type of flow in a channel is heavily dependent on the geometry through which the fluid is flowing and the transition from one flow type to another is determined experimentally and is distinguished for varying geometries at varying Reynolds numbers. The Reynolds number is a non-dimensional number dependent on the fluid properties, velocity and flow channel geometry, it allows for different fluids to conform to the same analysis. Different fluids will transform to turbulent behaviour at the same or very similar Reynolds numbers, for a given geometry. For flow over a flat plate the transitional Reynolds number is $Re \approx 2100$ [11]. The development length, is also relevant for flow through a channel, after which the boundary effects reach the centre of the channel and the resulting flow becomes uniform in nature.

Laminar Flow

Laminar flow is dominated by uniform streamlines, in the boundary layer where the fluid touches a surface the viscosity keeps the flow intact. The velocity of the fluid increases con-

tinuously away from the boundary layer. There is a continuum. There are no swirls, eddies or disruption in the flow.

Turbulent Flow

Turbulent flow begins as the inertial forces of the flow overcome the viscous forces, which then disrupts the flow. The uniformity of flow is disrupted in the boundary layer through the ‘transition’ phase between the laminar regime and turbulent regime. In the turbulent regime the inertial forces dominate the flow and the kinetic energy of the fluid results in eddies, swirls and vortices which characterise the flow. The viscous forces are no longer able to maintain a continuum. The transition phase between the two regimes can be unpredictable and difficult to model, as eddies and swirls break off in a chaotic manner.

Flow around a cylinder

As a fluid flows past a blunt object such as cylinder, flow separation is observed at remarkably low Reynolds numbers, $Re_{D_h} \geq 10$ [14]. This flow separation occurs as the flow can not follow the curved geometry of the cylinder past a separation point, which varies with the fluids kinetic energy. The inertial forces of the fluid are too strong for the effects of the boundary layer and a separation bubble is formed in the wake of the cylinder, which is characterised by an adverse pressure drop and the flow follows upstream behind the cylinder in a circular path, seemingly trapped.

Flow through a channel

Under normal circumstances, as a fluid flows through a channel an infinitesimal portion of the fluid directly in contact with the wall, sticks to the wall. This effect is described as a 'no-slip' condition. The viscous nature of the fluid drives this shear force deeper into the fluid and away from the wall. This leads to a parabolic velocity profile near the wall. If the viscosity of the fluid is strong enough or the channel is small enough this shear force will eventually dominate the flow and a 'fully developed flow' will form.

Hydrostatic diameter

For flow disrupted by an object or through a channel, one of the most important measurements is the hydrostatic diameter also known as the hydraulic diameter, which is a ratio of the wetted area to wetted perimeter of a geometry through which a fluid is moving in or around. It is commonly used in the determination of a non-dimensional numbers and is crucial for the determination of the Reynolds number upon which a lot of analysis relies. For flow between semi-infinite fins we find;

$$D_h = \frac{4 \text{ Area}}{\text{Perimeter}} = \frac{2ab}{(a+b)} = \frac{2a}{\frac{a}{b} + 1} = 2a \quad \left(\lim_{b \rightarrow \infty} \frac{a}{b} = 0 \right)$$

where, a = width , b = length

for flow around a cylinder the hydrodynamic length is given as; D_h = diameter of tube.

Thus, for our investigation we find the hydrostatic diameters for the types of flows we will deal with to be;

$$D_h (\text{ between fins }) = 2 (1.814) = 3.628 \times 10^{-3} \text{ m}$$

$$D_h (\text{ around pipe }) = 9.535 \text{ mm} = 9.5350 \times 10^{-3} \text{ m}$$

Another accepted hydrostatic diameter used in the analysis of condensers is given as

$$D_h = 4 \frac{A_c}{A_t} L \quad \text{where, } A_c = \text{ channel entrance area, [16]}$$

$$A_t = \text{ heat transfer area, } L = \text{ channel length.}$$

This form of the hydrostatic diameter will allow for variation between the proposed model and classical model.

Reynolds number

The Reynolds number is a common dimensionless number used in the description of flowing fluids and is often used in order to determine the type of fluid flow, given the geometry. It is a ratio of inertial to viscous forces. The Reynolds number is defined as;

$$Re = \frac{\rho v D_h}{\mu} \quad \text{where, } D_h = \text{ the hydrostatic diameter}$$

$$\mu = \text{ the dynamic viscosity}$$

$$v = \text{ the magnitude of velocity.}$$

The Reynolds number is highly dependent on the hydrostatic diameter, determined by the geometry as well as the fluid properties and velocity. The transition Reynolds number for flow through a channel is $Re_{D_h} \approx 2300$ [11] and in our investigation the Reynolds numbers are calculated to be;

$$491.0829 \leq Re_h(\text{ between fins }) \leq 1227.3 \quad \text{laminar flow regime}$$

$$1290.2 \leq Re_h(\text{ around pipes }) \leq 3225.6 \quad \text{turbulent flow regime.}$$

Fully Developed Flow

A fully developed flow in a channel is characterised by parallel streamlines in a similar fashion to laminar flow. This occurs as the viscous forces of the wall reach the centre of an enclosure through which the fluid is flowing. The flow is dominated by the viscous forces instituted through a no-slip boundary. This results in a parabolic velocity profile. There is a length scale that determines how far the fluid must travel through a channel before a fully developed flow is established, this is known as the hydrodynamic developing length or hydrodynamic entrance length. A turbulent hydrodynamic fully developed flow tends to flow faster towards the walls than a laminar hydrodynamic fully developed flow and results in a parabolic velocity profile that is steeper near the walls and flatter at its centre. The analytical calculation of the hydrodynamic entrance length for laminar flow through a semi-infinite duct it is given as;

$$L_h = C_h Re_{D_h} D_h \quad \text{where, } D_h = \text{ hydrostatic diameter}$$

the entrance length coefficient is experimentally determined to be $C_h = 0.011$ for flow between semi-infinite plates. Approximating the flow in-between the fins of our condenser as flow between semi-infinite plates, as the width \ll length, we discover that the developing length between the fins is between; $19.6 \text{ mm} \leq L_h \leq 48.7 \text{ mm}$. Thus, at the lower velocity the flow is fully developed before it interacts with the pipe and at the upper velocity the flow interacts with the pipe before it is fully developed.

CHAPTER 3

HEAT TRANSFER

Heat transfer is the objective of this study. Heat is a form of energy and as a consequence of the first law of thermodynamics, energy can not be created nor destroyed. Thus we seek the mechanisms by which the heat can be transferred and/or transformed into another form of energy. The predominant mechanisms at work in a condenser are conduction, convection and radiation. We consider each in turn here.

Conduction

Conduction is the transfer of heat through a material. Following from Fouriers law we find the differential form described in one dimension is;

$$q = -kA \frac{dT}{dx} \quad \text{where, } k = \text{thermal conductivity, a property of the material.}$$

Conduction is used in a tube fin condenser to move the heat out of the pipe, which then conducts heat through the fins, to then be convected away. The greater the conductivity of the material the more heat can be moved towards the convective fluid boundary. As such it is popular to use copper pipes as they are close to the heat source and have a good conductivity. Aluminium is often used for the fins due to its cost to conductivity ratio.

Convection

Convection is defined as the transfer of heat through mass transport. There are two different categories of convection, natural convection and forced convection. We find that following Newtons law of cooling, the convective heat transfer can be described mathematically as;

Surface Heat Transfer Number or Convective Heat Transfer Coefficient

$$h = \frac{q}{T_{wall} - T_{ref}} \quad \text{where, } h = \text{surface heat transfer coefficient}$$

$$T_{wall} = \text{temperature at the wall, } T_{ref} = \text{reference temperature.}$$

The surface heat transfer number plays a very significant role in the air-side cooling of a heat exchanger. It is the dominant variable which can be altered in order to increase the rate at which heat can be dissipated. In convection problems the convective heat transfer coefficient changes along the path of flow as the flux and temperatures difference is continually altered.

Natural convection occurs due to the heating effects on the cooling fluid, which causes the fluid to rise and an induced flow results due to the buoyancy force which comes from the difference in density of the heated and cooler surrounding fluid.

Forced convection occurs due to a pressure difference which is driven by an external force such as a fan or a pump. Forced convection is a more efficient cooling mechanism than natural convection as the temperature difference $T_{wall} - T_{ref}$ remains small. However it comes at the cost of powering a pressure inducing or reducing device. Forced convection is the primary driving force we are concerned with in compact heat exchangers, such as condensers.

Dimensionless numbers

Nusselt Number

The Nusselt number describes the ratio of convective heat transfer to conductive heat transfer, described as

$$Nu = \frac{hL}{k} \quad \text{where, } h = \text{ convective heat transfer coefficient}$$
$$k = \text{ thermal conductivity coefficient.}$$

As the thermal conductivity coefficient is a property of the material, while the convective heat transfer coefficient is a property of the instantaneous convective effects. The average nusselt numbers are often compared for analysis. A higher Nusselt number given the same materials will result in a higher average convective heat transfer number and higher heat transfer.

Prandtl Number

The Prandtl number describes the ratio of momentum diffusivity to conductive diffusivity and is given by;

$$Pr = \frac{\mu C_p}{k} \quad \text{where, } \mu = \text{ dynamic viscosity}$$
$$C_p = \text{ specific heat.}$$

The Prandtl number is a property of the material and its temperature.

Radiation

Radiation is described mathematically as;

$$q = \epsilon A (T_{wall}^4 - T_{ref}^4) \quad \text{where, } \epsilon = \text{the emissivity, a property of temperature and material.}$$

$q =$ heat transfer flux.

Due to the low emissive and absorptive quality of air, and the close proximity of temperature between the fins the radiative effects are negligible compared to the conductive and convective effects undergone by the airside cooling of a condenser. Thus, we ignore the radiative effects in this investigation.

As a note we also ignore friction heating, as it too is a mechanism that has negligible effect.

CHAPTER 4

MATHEMATICAL FORMULATION

To simulate the physical effects of forced convection on the air-side heat transfer condenser, we formulate equations around three conservation laws of physics. The conservation of mass, the conservation of momentum and the conservation of energy. These general laws must then be placed into the form of equations which can be solved.

Conservation of Mass

The conservation of mass stipulates that mass can not be created or destroyed. It is described mathematically as the continuity equation;

$$\frac{\partial \rho}{\partial t} + \nabla \cdot (\rho \vec{v}) = 0 \quad \text{where, } \rho = \text{fluid density, } \vec{v} = \text{fluid velocity vector.}$$

for gas flows where the Mach number, which is the ratio of the fluids velocity to the speed of sound in the fluid is less than 0.3, it is always safe to assume the density is constant [2] and the conservation of mass equation leads to: $\nabla \cdot \vec{v} = 0$.

Conservation of Momentum

The conservation of momentum is Newton's second law. Force is equal to the change in momentum per unit time. It is described mathematically as;

$$F = m\vec{a} = \frac{d}{dt}(m\vec{v}) \quad \text{where, } F = \text{force, } m = \text{mass.}$$

When applied to Newtonian fluids this leads to a set of equations called the Navier-Stokes equations. Assuming constant density and viscosity the Navier-Stokes equations reduce further to [11]

$$\rho \frac{D\vec{v}}{Dt} = \rho\vec{g} - \nabla p + \mu\nabla^2\vec{v} \quad \text{where, } \vec{g} = \text{gravity vector, } g = \text{gravity magnitude.}$$

$$\rho \left(\frac{\partial\vec{v}}{\partial t} \right) + \rho(\vec{v} \cdot \nabla)\vec{v} = -\nabla p + \mu\nabla^2\vec{v} + \rho g \quad \mu = \text{fluid dynamic viscosity.}$$

given in cartesian coordinates as;

$$\rho \left(\frac{\partial u}{\partial t} + u \frac{\partial u}{\partial x} + v \frac{\partial u}{\partial y} + w \frac{\partial u}{\partial z} \right) = \rho g_x - \frac{\partial p}{\partial x} + \mu \left(\frac{\partial^2 u}{\partial x^2} + \frac{\partial^2 u}{\partial y^2} + \frac{\partial^2 u}{\partial z^2} \right)$$

$$\rho \left(\frac{\partial v}{\partial t} + u \frac{\partial v}{\partial x} + v \frac{\partial v}{\partial y} + w \frac{\partial v}{\partial z} \right) = \rho g_y - \frac{\partial p}{\partial y} + \mu \left(\frac{\partial^2 v}{\partial x^2} + \frac{\partial^2 v}{\partial y^2} + \frac{\partial^2 v}{\partial z^2} \right)$$

$$\rho \left(\frac{\partial w}{\partial t} + u \frac{\partial w}{\partial x} + v \frac{\partial w}{\partial y} + w \frac{\partial w}{\partial z} \right) = \rho g_z - \frac{\partial p}{\partial z} + \mu \left(\frac{\partial^2 w}{\partial x^2} + \frac{\partial^2 w}{\partial y^2} + \frac{\partial^2 w}{\partial z^2} \right)$$

Where, u, v and w are the x, y and z component of the velocity respectively and g_x, g_y, g_z are the x, y and z component of gravity. To date a mathematical proof for the existence and smoothness of a solution for the Navier-Stokes equations has not been found and a bounty of \$1 million has been offered by the Clay Mathematics Institute as part of their millennium problem competition and has been on offered since the year 2000.

More information and a copy of the millennium problem statement can be found at; <http://www.claymath.org/millennium-problems/navier-stokes-equation>

Conservation of Energy

The conservation of energy formulation comes from the first law of thermodynamics. Energy can not be created nor destroyed and can only be converted from one form of energy to another form of energy. It is described as;

$$\left[\begin{array}{l} \text{Change in internal} \\ \text{and kinetic energy} \end{array} \right] = \left[\begin{array}{l} \text{rate of internal and kinetic energy} \\ \text{transport via convection} \end{array} \right] + \left[\begin{array}{l} \text{rate of heat energy added} \\ \text{by conduction} \end{array} \right] - \left[\begin{array}{l} \text{rate of work done} \\ \text{by the surroundings} \end{array} \right]$$

$$\rho C_p \frac{DT}{Dt} = \nabla \cdot k \nabla T + \beta T \frac{Dp}{Dt} + \mu \phi \quad \text{where, } \phi = \text{dissipation function, } T = \text{temperature,}$$

$$\phi = 2 \left[\left(\frac{\partial u}{\partial x} \right)^2 + \left(\frac{\partial v}{\partial y} \right)^2 + \left(\frac{\partial w}{\partial z} \right)^2 \right]$$

$$+ \left[\left(\frac{\partial u}{\partial y} + \frac{\partial v}{\partial x} \right)^2 + \left(\frac{\partial v}{\partial z} + \frac{\partial w}{\partial y} \right)^2 + \left(\frac{\partial w}{\partial x} + \frac{\partial u}{\partial z} \right)^2 \right] - \frac{2}{3} \left(\frac{\partial u}{\partial x} + \frac{\partial v}{\partial y} + \frac{\partial w}{\partial z} \right)^2$$

$$\beta = -\frac{1}{\rho} \left[\frac{\partial \rho}{\partial T} \right]_p = \text{coefficient of thermal expansion.}$$

Reynolds Averaged Navier Stokes Equations (RANS)

The Reynolds Averaged Navier Stokes Equations, refer to a set of equations that solve the Reynolds decomposition of the Navier Stokes equations. For turbulent flows at any point in the flow it is noticeable that the velocity fluctuates with time. Thus Reynolds proposed decomposing

the velocity into two components, the sum of mean values of the velocity and the fluctuation.

$$\vec{v} = \bar{v} + v' \quad \text{where, } \bar{v} = \int_{t-\frac{1}{2}t_0}^{t+\frac{1}{2}t_0} \vec{v}(s) ds$$

$$\overline{v'} = 0, \quad \overline{\bar{v}} = \bar{v} \quad \overline{v'\bar{v}} = 0, \quad \overline{\frac{\partial}{\partial x} \vec{v}} = \frac{\partial}{\partial x} \bar{v}, \quad \overline{\frac{\partial}{\partial t} \vec{v}} = \frac{\partial}{\partial t} \bar{v}.$$

the same is done for pressure and the relations are then used in the Navier-Stokes equations for constant density, leading to the Reynolds averaged continuity and Navier-Stokes equations;

The continuity equation is;

$$\nabla \bar{v} = 0$$

The momentum conservation equation is;

$$\rho \frac{D\bar{v}_i}{Dt} = F_i - \frac{\partial \bar{p}}{\partial x_i} + \mu \nabla^2 \bar{v}_i - \rho \left(\frac{\partial \overline{v'_i v'_j}}{\partial x_j} \right)$$

The energy conservation equation is;

$$\frac{\partial}{\partial x} (\rho C_p T u_i) = -\frac{\partial}{\partial x_i} \left(-k \frac{\partial T}{\partial x_i} + \rho C_p \overline{u'_i T'} \right)$$

After introducing additional variables to the analytical conservation equations, the RANS model requires additional equations in order to close the problem. There are several different models or sets of equations that have been developed to solve the RANS model without any specific universally accepted model for every problem. Rather each model has a specific sub-set of problems for which it will be superior to others. The choice of equation sets used to model a particular problem

is dependent on the time constraints, computational power as well as the flow regime and geometry through which the flow is moving through or over. Some of the most popular and economical equation models are the Spalart-Allmaras One-equation model, the $\kappa - \epsilon$ model, and the $\kappa - \omega$ model each of which have their own variational equations as well. Choice of an equation set to model a specific problem usually comes from experimental work and or a flow comparative study. For our simulations we chose the $\kappa - \omega, SST$ (Shear Stress Transition) equations as there is suggestion within the literature that this form of the $\kappa - \omega$ equations would be a suitable choice. [18] [13] [8][3].

$\kappa - \omega, SST$ equations.

The decision to use the $\kappa - \omega, SST$ equations for our investigation, has much to do with previous work in the field [18]. The $\kappa - \omega, SST$ equations are known to be robust in the transient phase, and for our initial investigations predicting laminar flow building to a fully developed profile through the fin channel and then detached flow forming turbulent behaviour in the wake of the pipes. The $\kappa - \omega, SST$ are the best choice as they resolve transient turbulent activity within the boundary layer, and as the flow detaches the SST formulation of the $\kappa - \omega$ equations begins to trend towards the $\kappa - \epsilon$ equations which resolve larger eddy for a fully turbulent flow. It has been shown that the $\kappa - \omega, SST$ 2 equation solution to the RANS model is a good choice for flow through the air-side of a condenser [13] [8]. The equations are given as;

$$\frac{\partial(\rho k)}{\partial t} + \frac{\partial(\rho U_i k)}{\partial x_i} = \bar{P}_k - \beta^* \rho k \omega + \frac{\partial}{\partial x_i} \left[(\mu + \sigma_k \mu_t) \frac{\partial k}{\partial x_i} \right]$$

$$\frac{\partial(\rho \omega)}{\partial t} + \frac{\partial(\rho U_i \omega)}{\partial x_i} = \alpha \rho S^2 - \beta \rho \omega^2 + \frac{\partial}{\partial x_i} \left[(\mu + \sigma_\omega \mu_t) \frac{\partial \omega}{\partial x_i} \right] + 2(1 - F_1) \rho \sigma_{\omega 2} \frac{1}{\omega} \frac{\partial k}{\partial x_i} \frac{\partial \omega}{\partial x_i}$$

$$F_1 = \tanh \left[\left(\min \left[\max \left(\frac{\sqrt{k}}{\beta^* \omega y}, \frac{500v}{y^2 \omega} \right), \frac{4\rho \sigma_{\omega 2} k}{CD_{k\omega} y^2} \right] \right)^4 \right]$$

$$CD_{k\omega} = \max \left(2\rho \sigma_{\omega 2} \frac{1}{\omega} \frac{\partial k}{\partial x_i} \frac{\partial \omega}{\partial x_i}, 10^{-10} \right) \quad y = \text{distance to closest wall}$$

We find that, $F_1 \rightarrow 0$, away from the surface as the model tends to ($k - \epsilon$ model), and $F_1 \rightarrow 1$ inside the boundary layer ($k - \omega$ model)

The turbulence eddy viscosity is defined as

$$v_t = \frac{a_1 k}{\max(a_1 \omega, SF_2)} \quad S = \text{invariant measure of the strain rate}$$

$$F_2 = \tanh \left(\left[\max \left(\frac{2\sqrt{k}}{\beta^* \omega y}, \frac{500v}{y^2 \omega} \right)^2 \right] \right)$$

To prevent the build up of turbulence in stagnation regions, there is a production limiter

$$P_k = \mu_t \frac{\partial U_i}{\partial x_j} \left(\frac{\partial U_i}{\partial x_j} + \frac{\partial U_j}{\partial x_i} \right) \rightarrow \bar{P}_k = \min(P_k, 10\beta^* \rho k \omega)$$

The constants are computed from a mix of the $k - \epsilon$ and the $k - \omega$ models.

$$\alpha = \alpha_1 F + \alpha_2 (1 - F), \text{ etc...} \quad \text{where,}$$

$$\beta^* = 0.09, \alpha_1 = \frac{5}{9}, \alpha_2 = 0.44, \beta_1 = \frac{3}{40}, \sigma_{k1} = 0.85, \sigma_{k2} = 1, \sigma_{\omega1} = 0.5, \sigma_{\omega2} = 0.856$$

The main modification from the standard $\kappa - \omega$ equations is the use of the strain rate S instead of vorticity in the turbulence eddy viscosity equation, and half the factor in \bar{P}_k [13]

CHAPTER 5

CFD SIMULATION

Finite Volume Method

The finite volume method is a discretised method of solving partial differential equations. It is known to be particularly robust for solutions involving the conservation equations, as the fluxes are locally conserved on each cell. The method is based on balancing the equations over each 'finite volume'. Gauss's divergence theorem is used to convert the volume integral of the divergence to a surface integral or flux. This flux is conserved over each cell with respect to the unknown variable and the resulting solution will have a finite residual error, which one seeks to minimise. [7]

Geometry

The design for the airside condenser was inspired by the experimental work of Lee et al. [22]. Lee, et al. proposed that by varying the number of pipe rows at different positions along the cooler one can obtain a more efficient system. They used industrial standard piping and flat plate fins. The properties of the fins are simulated as aluminium and the properties of the pipes are simulated as copper. The dimensions of the tubes and their spacing as well as a picture of the condenser is given in figure 1.

The condenser used by Lee et al, has both two pipe row and three pipe row configurations. Some of our initial investigations used two row configurations. Our final investigations were based on a



Table 1 – Physical dimensions of condenser coils.

Fin and tube heat exchanger configuration		
Length (L)	1470	mm
Height (H)	609.6	mm
Tubes for outer coil and inner coil	144	–
Vertical tube spacing	25.4	mm
Horizontal tube spacing	22.0	mm
Fin thickness	0.12	mm
Fins per inch	14	–
Outside tube diameter	9.535	mm
Tube thickness	0.356	mm

Figure 1: Left: a photograph of the chiller used in the experimental paper by Lee et al. Right: the dimensions of the chiller used in Lee et al. [22]

three row deep model.

Classical Model

We conduct a simulation on what we term the ‘classical model’, as a comparison for the altered condenser air side geometry of this study. Due to the symmetry of a flat plate condensers design and the need for a fine mesh, it was decided to create a single flow channel between two fins, for our model. Although the condenser designs in Lee at al, have both two rows and three rows of pipes in their design, our design uses a three row configuration this lends itself to a greater understanding of the flow through the channel and around the pipes.

In figure 2 and 3, we show a close up view of the classic and proposed models respectively. The mesh in each figure is without the fluids and top fin. Three planes of velocity contours have been added and one can notice the difference between the proposed model 3, with the vortex generator and the classic model 2 without the vortex generators.

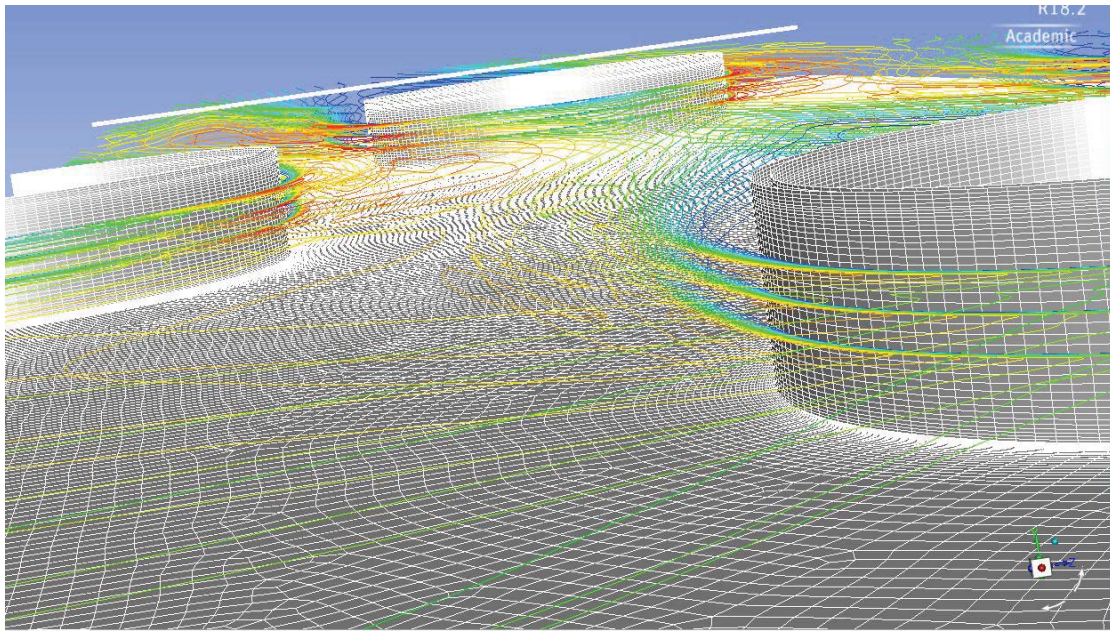


Figure 2: A close up view of the classic model, with flow lines

Proposed Model

Our proposed model design has the same structure and dimensions as the classical model. We add a vortex generator to either side of the pipes in order to stimulate flow in the region behind the pipes and remove the heat trapped there. It was thought the design of these vortex generators should be simple with both cost and feasibility of construction in mind. The vortex generators are designed of the same material (aluminium) and width as the fins. This would allow the vortex generators to be cut from the same roll of aluminium as the fins. We imagine the proposed model to be constructed by creating small insertions in the fins and then inserting a 'vortex generator' the length of the pipe, through the insertions and perpendicular to the fins. The breadth of our 'vortex generators' is created to be the length of the pipes diameter. We placed each vortex generator with its stagnation point in line with the centre of the pipe and perpendicular to the flow, 1 mm away

from the outer diameter of the pipe. The vortex generator is then angled inwards at a streamwise 10 degree angle, towards the separation area behind the pipe.

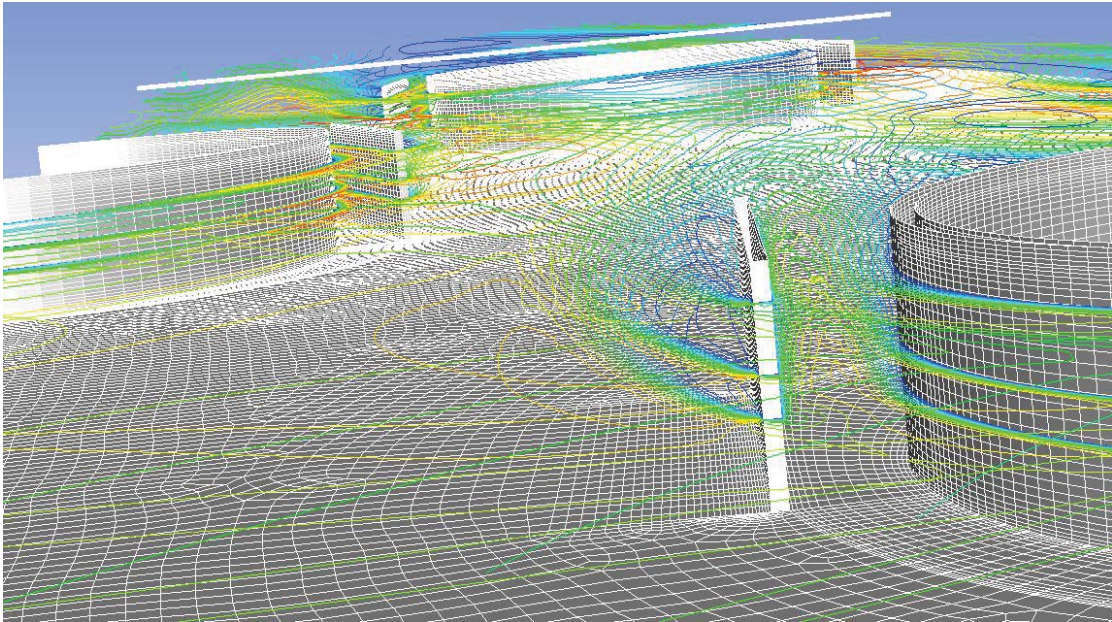


Figure 3: A close up view of the proposed model, with flow lines

Mesh

In constructing the mesh attention was paid to wall Y^+ value, as the $\kappa - \omega$ equations resolve the boundary layer, this demands that the Y^+ value ≤ 1 . The Y^+ value is a dimensionless number

defined as

$$Y_+ = \frac{\rho u y}{\nu} \quad \text{where, } y = \text{distance to the closest wall}$$
$$\nu = \text{kinematic viscosity}$$
$$u = \sqrt{\frac{\tau_w}{\rho}} = \text{wall stress, } \rho = \text{density}$$

It described a ratio of cell to wall stress and is a determinant of the boundary layer. In the use of most turbulent solutions where the turbulence is assumed to be fully developed the Y_+ value is recommended to be $30 \leq Y_+ \leq 300$. But the $\kappa - \omega$ equations need to resolve the flow within the boundary layer and thus it is recommended that the $Y_+ \leq 1$. Therefore, in our construction of the mesh, it is finer in regions closer to the wall. This also results in a larger aspect ratio, which is the length the height or width ratio of a quadratic cell. Large aspect ratios can lead to difficulties with convergence.

We constructed each fin 4 cells deep in order to allow for the conduction through the fins to be properties to resolved, while the pipes are each 5 cell elements thick. The mesh was constructed of mostly quadratic elements were possible with the hexacore meshing procedure in the Ansys Fluent meshing programme. [3]

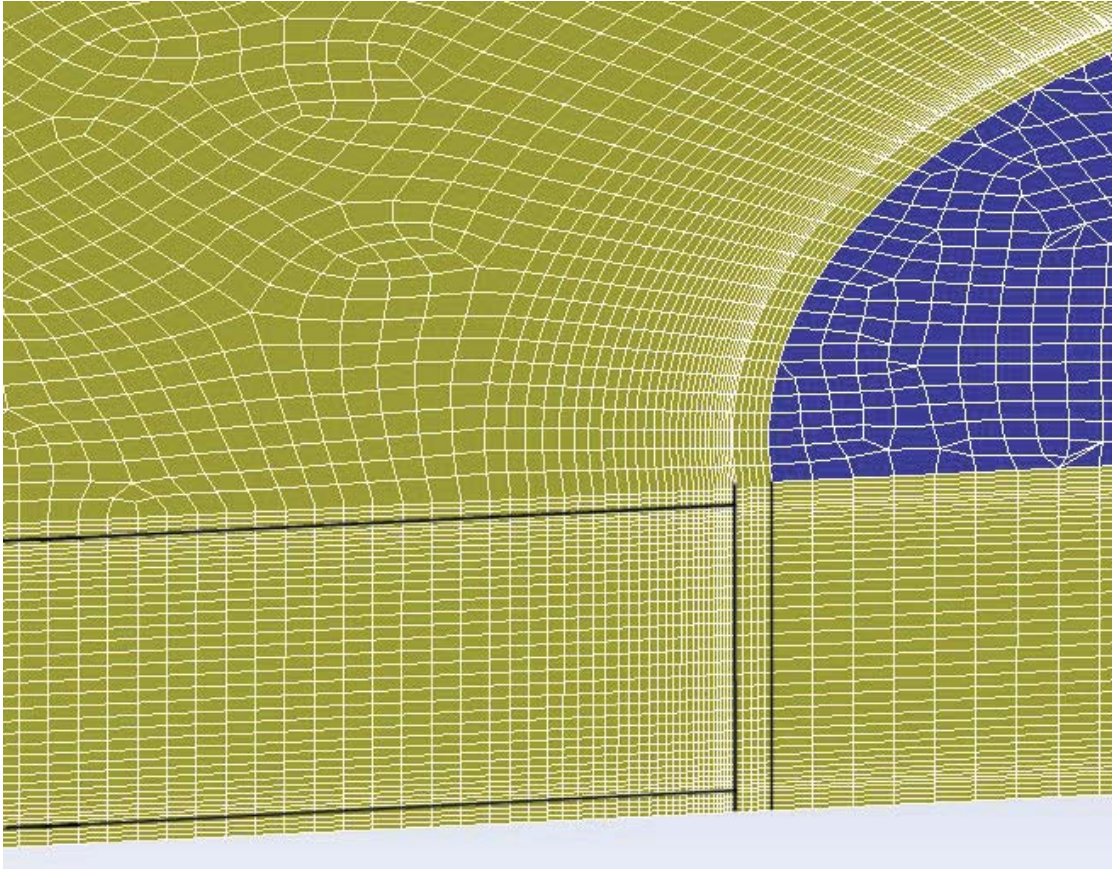


Figure 4: A partial view of the mesh

In figure 4 we see a part of the mesh design where the fins meet one of the pipes. One can notice that the cells are mostly hexahedral and as the the mesh draws towards a boundary between the fins, air or pipe, the mesh gets finer in order to satisfy the Y^+ condition to resolve the $k - \omega$ equations. The water defined in figure 4 occupies the mesh below the highlighted blue area. The water-pipe boundary does not have a growth as the flow within the pipe is defined as laminar. The growth seen in the top and bottom of the water zone is a consequence of the automatic meshing algorithm and the want for a uniform mesh.

Convergence

We ran a mesh independence study on 4 mesh sizes, from 2 065 797 nodes to 5 775 276 nodes. The mesh was focused more compactly through the solid geometry with attention paid to the y+ wall values, the outlet was extended to over half the length of the model in order to avoid numerical back flow issues arising from the adverse pressure conditions of the flow around the pipe. In instances with a shorter flow exit region, Fluent defines the flow on certain elements instead of calculating them in order to satisfy the mass flow rate. The material properties were defined as default by Fluent. The simulations we ran are pressure based models, which allowed us to set the magnitude of the inlet flow velocity and temperature (293.15K (20°C), $|\vec{v}|$). The simulation maintains a static pressure at the exit area at 0 Pa. The algorithm chosen was ‘SIMPLE’ with Second Order equations for both energy and motion. We judged convergence based on both the residual and a flux balance. The residuals achieved all fell below 10^{-4} , while the residuals for the energy equation were all below 10^{-9} . Checking the convergence through a heat flux balance showed negligible error in all simulations, with an outward mean heat flux of order 10^3 the balance was found to be between 10^{-6} and 10^{-8} .

Area-Weighted Average Total Surface Heat Flux	(w/m2)	Area-Weighted Average Total Surface Heat Flux	(w/m2)
interior-fin_1-pipes	-263579.21	interior-fin_1-pipes	-293853.47
interior-fin_1-pipes-shadow	263579.21	interior-fin_1-pipes-shadow	293853.47
interior-fin_2-pipes	-262743.77	interior-fin_2-pipes	-293077.95
interior-fin_2-pipes-shadow	262743.77	interior-fin_2-pipes-shadow	293077.95
wall-air_enter-fin_1	-2486.4911	wall-air_enter-fin_1	-2385.0449
wall-air_enter-fin_1-shadow	2486.4911	wall-air_enter-fin_1-shadow	2385.0449
wall-air_enter-fin_2	-2477.4785	wall-air_enter-fin_2	-2375.6221
wall-air_enter-fin_2-shadow	2477.4785	wall-air_enter-fin_2-shadow	2375.6221
wall-air_exit-fin_1	-573.62103	wall-air_exit-fin_1	-691.39908
wall-air_exit-fin_1-shadow	573.62083	wall-air_exit-fin_1-shadow	691.39778
wall-air_exit-fin_2	-569.67259	wall-air_exit-fin_2	-686.11563
wall-air_exit-fin_2-shadow	569.67239	wall-air_exit-fin_2-shadow	686.11692
wall-air_main-fin_1	-1401.7451	wall-air_main-fin_1	-1563.1142
wall-air_main-fin_1-shadow	1401.7451	wall-air_main-fin_1-shadow	1563.1142
wall-air_main-fin_2	1397.3068	wall-air_main-fin_2	1559.257
wall-air_main-fin_2-shadow	-1397.3068	wall-air_main-fin_2-shadow	-1559.257
wall-air_main-pipes	-2639.5493	wall-air_main-pipes	-3002.8385
wall-air_main-pipes-shadow	2639.5493	wall-air_main-pipes-shadow	3002.8385
wall-pipes-water	36320.343	wall-pipes-water	40556.744
wall-pipes-water-shadow	-36320.343	wall-pipes-water-shadow	-40556.745
Net	-4.1911521e-07	Net	-2.0862614e-06

Figure 5: Balance of heat flux over all surfaces Left: velocity 2.5 m/s Right: velocity 3.0 m/s

In figure 5 a flux balance is shown on two different models. A calculation on the area-weighted average total surface heat flux, $\frac{1}{A} \sum_{i=1}^n q_i |A_i|$ [3]. We notice that the average on each surface is of the order of $10^3 - 10^5$ while the net average is of the order $10^{-6} - 10^{-7}$.

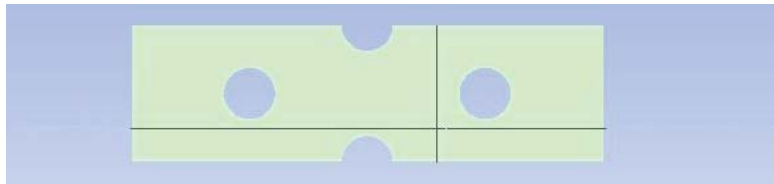


Figure 6: grid independence profile lines

Figure 6 represents the two lines through the mid-plane on which we conducted the grid independence study, using both the velocity magnitude and static temperature.

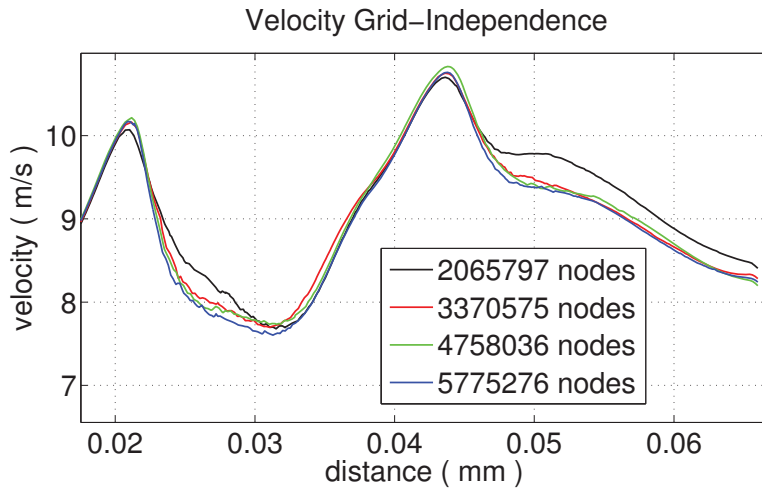
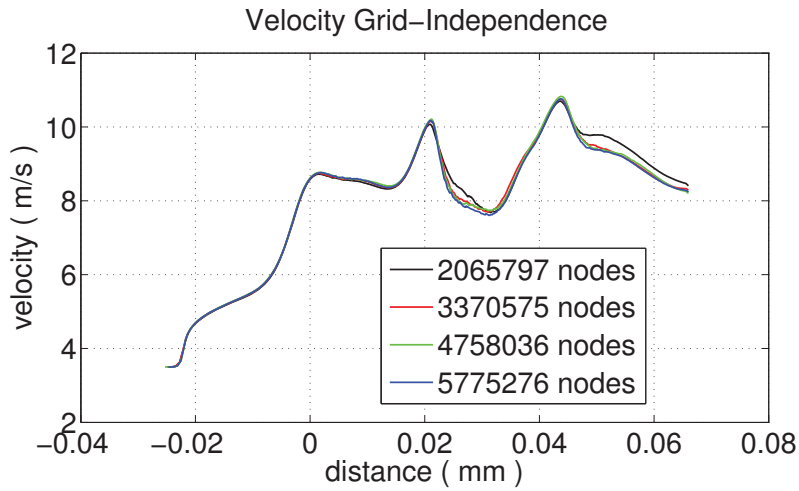


Figure 7: grid independence plots of velocity along the length of our geometry.

In figure 7 we show the velocity profiles along the length of the geometry. The lower graph highlights the points where the meshes vary from one another and we note a minimal difference between the 5 million node mesh and 4 million node mesh compared to the 2 million node mesh, which becomes more prevalent in the temperature profile.

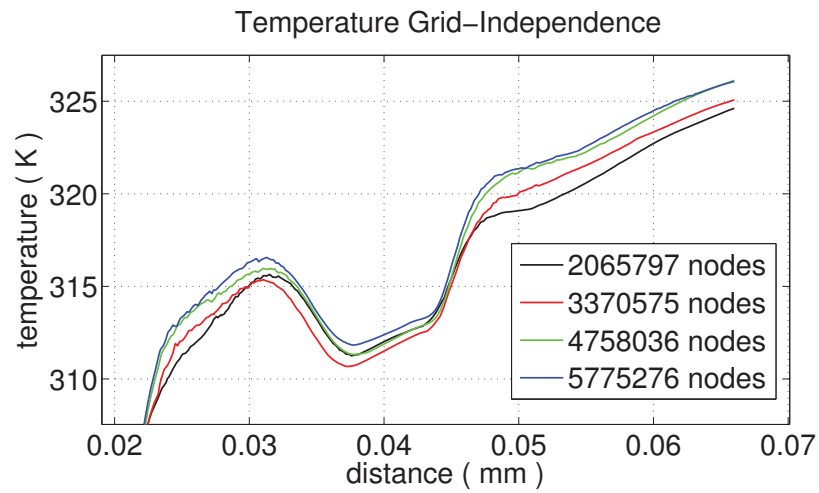
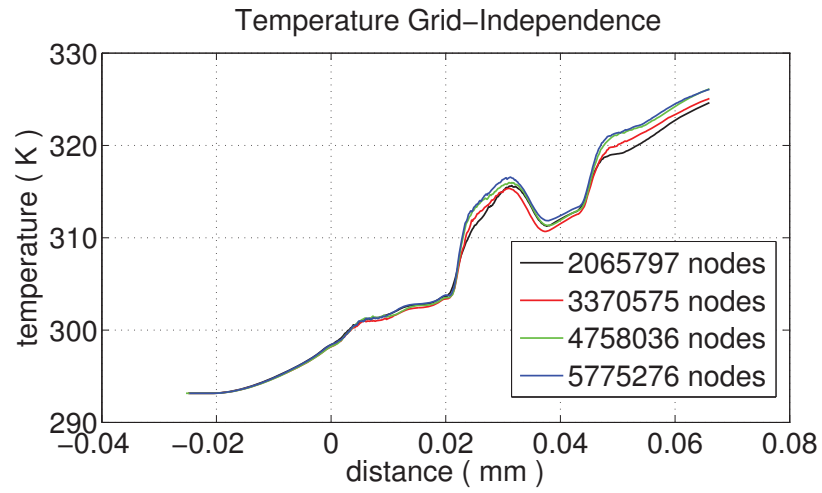


Figure 8: grid independence plots of the temperature along the length of our geometry.

In figure 8 we show the temperature profiles along the length of the geometry. The lower graph highlights the points where the meshes vary from one another and we note a minimal difference between the 5 million node mesh and 4 million node mesh compared to the 2 million node mesh.

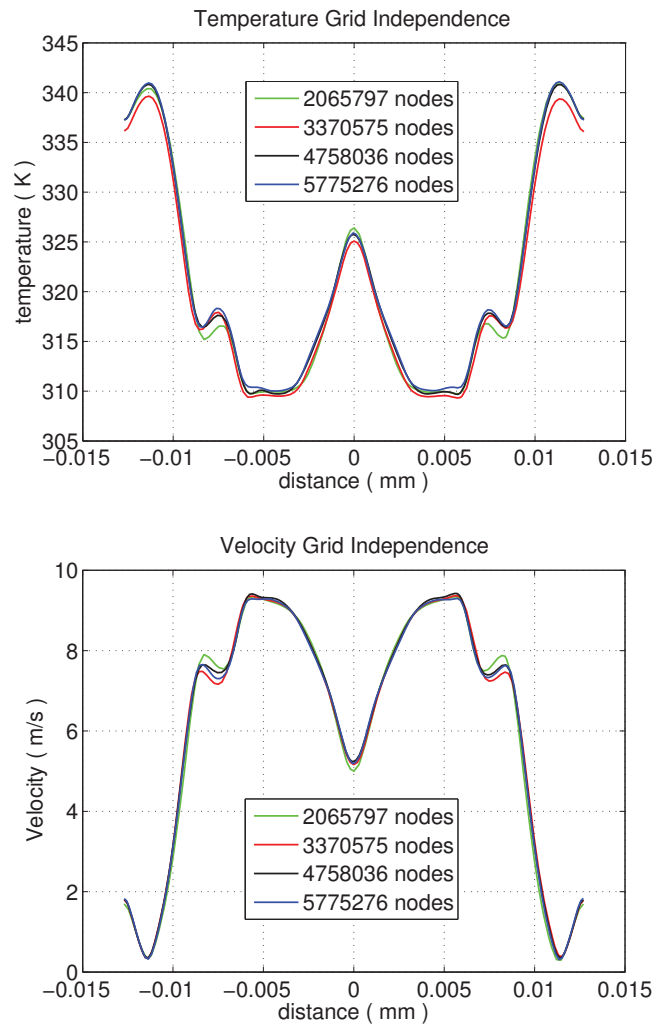


Figure 9: grid independence plots of temperature and velocity along the width of our geometry. Top: Velocity profile. Bottom: Temperature profile.

Set-Up

After creating the specific geometries in Ansys SpaceClaim and refining them in Ansys design modeller we ran the simulations using Ansys Fluent. Choosing the working fluids as water within the pipes and air through the air-side flow channel. The pipes were given the properties of copper while the fins are set as aluminium. This mean the boundary between the pipes and fins are set

as a 'wall' as apposed to 'internal'. All the fluid to pipe, vortex generator and fins we set as 'wall's. The boundaries of the simulation were set as 'symmetry'. The heat was generated in the pipes by simulating water flow at 0.1 m/s and at a temperature of 353.15K (80°C) through the inlet of each pipe. The air-side flow was set at various flow velocities and at a temperature of 293.15K (20°C). We mostly ran the 'coupled algorithm' configuration in our simulations and left them to run overnight with a courant flow number of 25, lowering that number as well as some of the under-relaxation factors to achieve a suitable convergence and low residual. It was found that running the 'coupled algorithm' simulations and manually lowering the courant numbers led to the best convergence with lowest residual output. The simulations were also found to be quite sensitive to the respective under-relaxation factors.

CHAPTER 6

ANALYSIS

Convective Influence

The convective influence on the augmentation of both the classical and proposed condenser models are demonstrated through the mid-plane velocity and temperature contours and graphs of the air passing through the flow channel. The mid-plane view reveals a significant analysis of the augmentation as the mid-plane regions flow is the least effected by the fin-wall boundaries and will also have the coolest temperatures. In the figures 10 and 11 we present profiles of the air temperature and velocity magnitude through the lines presented at the top of the figures that run perpendicular to the flow through the mid-plane. Data from both the classic and proposed models of the velocity magnitude and temperature for each node along the line are presented together. The data is gathered from simulations with a 3 m/s face velocity.

It is interesting to note the inverse relationship between the temperature and velocity fields, showing how the magnitude of the air velocity as it passes through the condenser channel significantly effects the convective cooling.

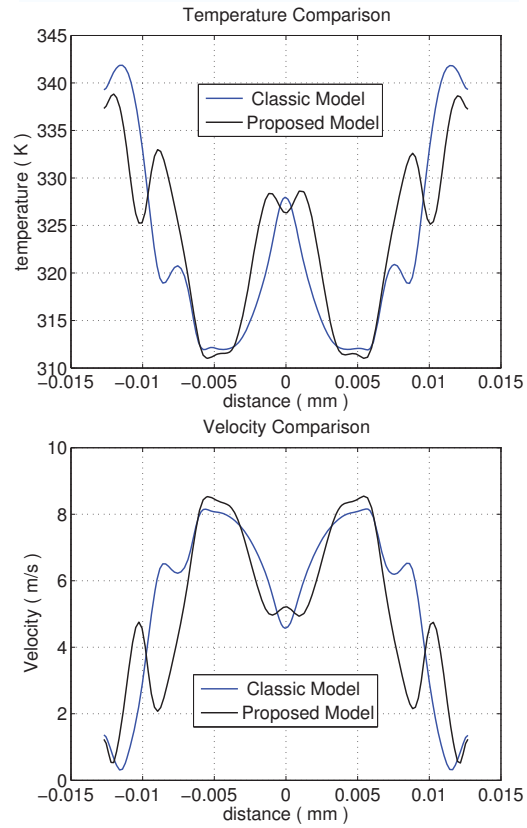
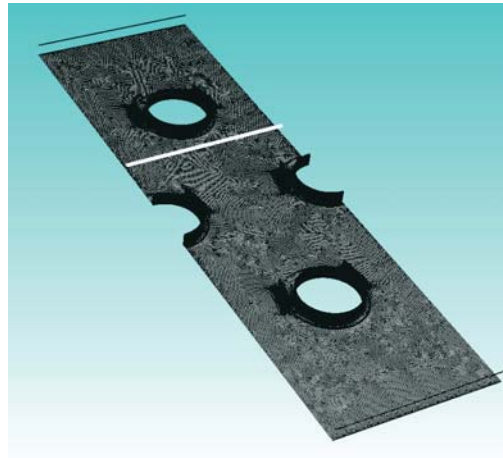


Figure 10: Top: Graphic showing the line along which the profiles are taken with an entrance velocity of 3m/s. Middle: Temperature profiles of classic and proposed model along line Bottom : Velocity profiles of classic and proposed model along line.

In figure 10 the profile line is close to the front or stagnant point of the pipe in the 3rd row. We notice that the temperature is hottest at the sides of the temperature plot, as the air temperature is affected by the pipes in the second row. The temperature of the proposed model is lower than that of the classic model as the air in the proposed model is being disrupted in this region by the vortex generators. Interestingly the temperature is seemingly inversely proportional to the velocity and at the sides of this plot we find that the proposed model has a slightly lower velocity than the classical model as well as a more pronounced lower temperature than the classical model. Using Reimann sums to find the average temperature; $\sum f(x_i) |x_{i+1} - x_i| \times |x_1 - x_{end}|$. We find the average temperature of the proposed model in 10 is, 323.8 K and the average temperature of the classic model in 10 is, 322.6 K.

In figure 11 we have a similar profile plot to figure 10 going through a line just behind the first row of pipes. In this profile it is noticeable that in the region behind the pipe the proposed model has lower temperatures, which was the aim of our design. To move the stagnant and intensely heated air behind the pipes. There is also a very noticeable ‘bump’ in the temperature of the proposed model around 0.005 mm, which we assume is caused by the wake of the vortex generators which are also conducting heat through its surface. The Riemann sums analysis for the average temperatures in 11 yield an average temperature for the proposed model of; 315.9 K and an average temperature of the classic model of 315.8 K.

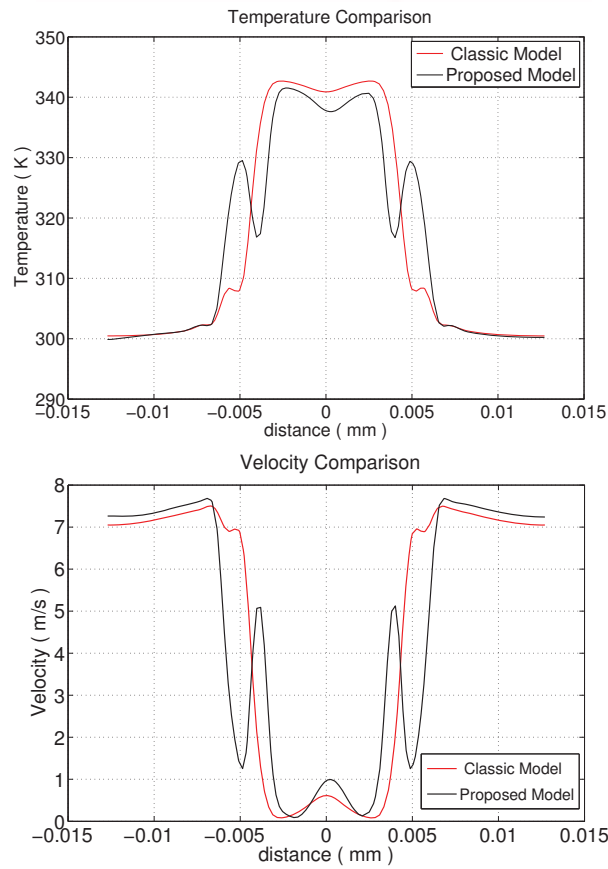
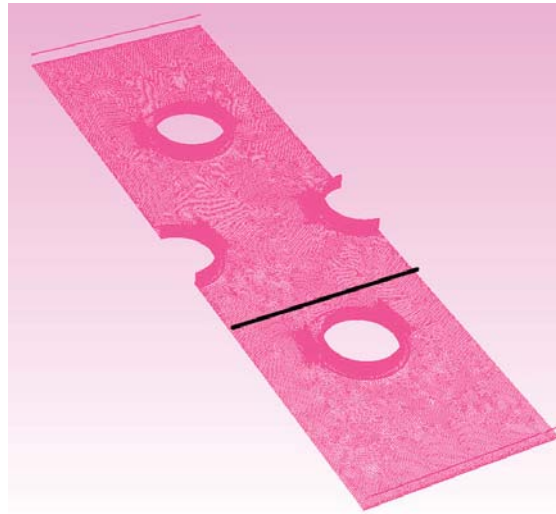


Figure 11: Top: Graphic showing the line along which the profiles are taken with an entrance velocity of 3m/s. Left: Temperature profiles of classic and proposed model along line. Right: Velocity profiles of classic and proposed model along line.

Through the mid-plane contour plots, figure 12, and figure 13 we show the velocity and temperature contours of the classical model next to and to the left of the proposed model for the face entrance velocities; 3.0 m/s, 3.5 m/s, 4.0 m/s and 5.0 m/s.

The velocity contours in figure 12, describe how the vortex generators effect the flow through the channel, particularly in the wake region immediately behind the pipes where there is a significantly smaller region of stagnant air. It can also be seen that towards the sides of the pipes and parallel to the flow, the velocity magnitude of the proposed model is greater than that of the classical model. From the discussion surrounding figure where we see the temperature seemingly inversely proportional to the velocity magnitude, this increase in velocity will result in a lower temperature in that region. Following the flow through the proposed model that is being forced by the vortex generators to travel further around the pipes before turbulent shedding occurs, it is reasonable to assume that a good portion of the stagnant heated air is being moved. The differences in the velocity magnitude and size of the stagnation areas between the classical models and proposed models trend to increase with an increase in the face velocity. As the stagnation area is where a lot of heat is being kept, it is reasonable to conclude that the larger the difference in these areas between the two models, the larger the effectiveness of the proposed model. Thus, we could predict that higher face velocities will lead to higher efficiencies.

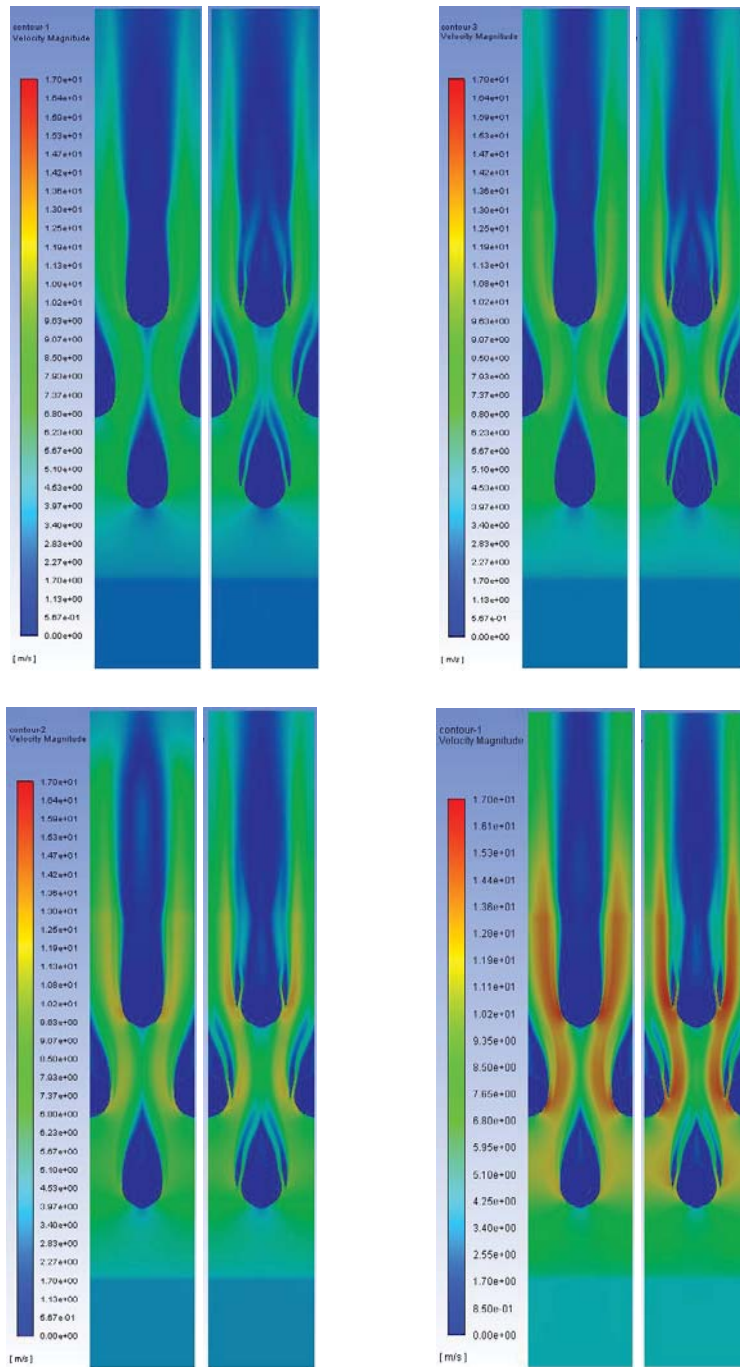


Figure 12: Mid-plane velocity contours with entrance velocities Top Left: 3.0m/s. Top Right: 3.5m/s. Bottom Left: 4.0m/s. Bottom Right: 5.0 m/s.

In the temperature mid-plane contours, figure 13. It is noticeable that the temperatures in the wake of all the pipes is higher at lower face velocities. This is to be expected as the heat is transported more slowly at lower face velocities and the air has more time to draw and absorb the heat from the condenser. It is also noticeable when comparing the classical model and proposed model at the same face velocities, that the 'wake of heat' in the region behind of the 3rd row pipe of the proposed models extends further out than the classical models. This longer wake is a sign of more heat leaving the model. It is also noticeable that the pipes in the proposed model are more defined as the cooler air coloured green travels further around the pipe. In the wake of the first row pipe we notice that the heat is broken up more by the proposed model, and this become even more evident at the higher face velocities. It is evident in the mid-plane that there is more heat being transported in the proposed model than the classic model.

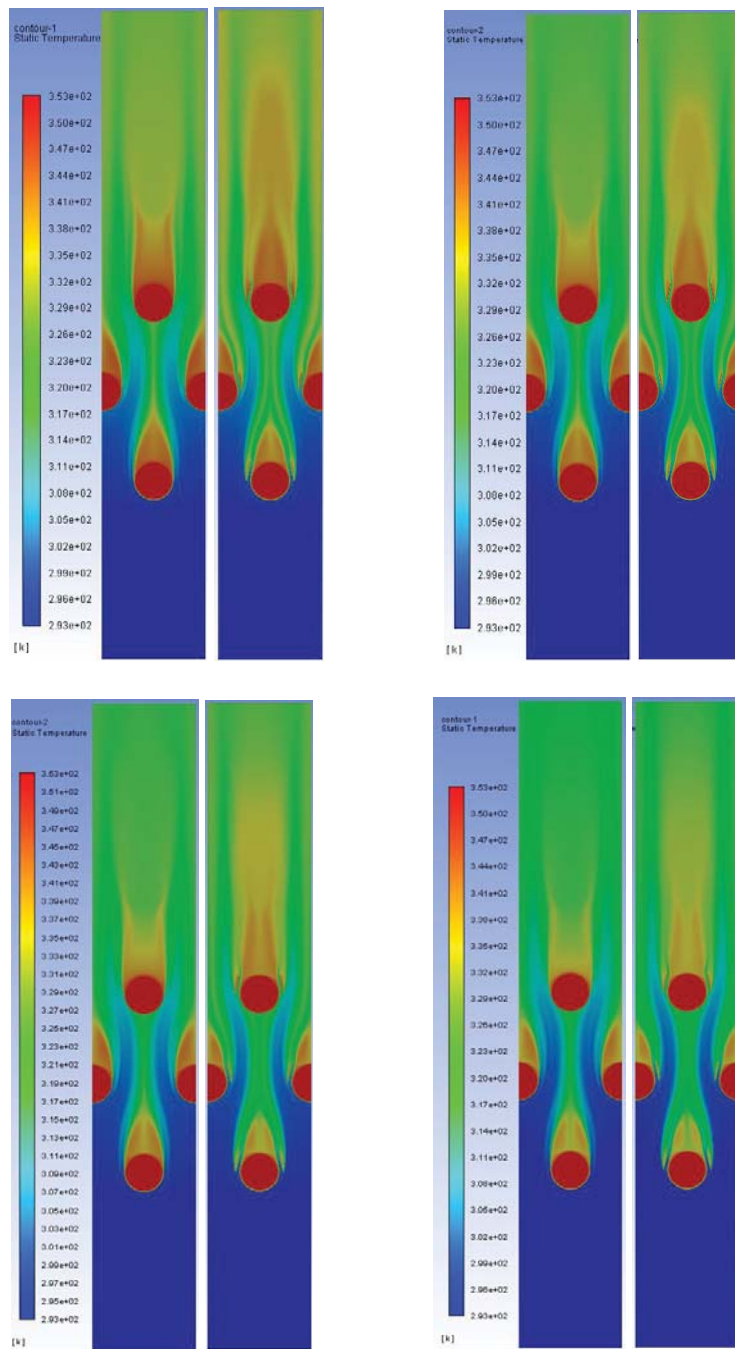


Figure 13: Mid-plane temperature contours with entrance velocities Top Left: 3.0 m/s. Top Right: 3.5 m/s. Bottom Left: 4.0 m/s. Bottom Right: 5.0 m/s.

Conductive Influence

It is also relevant to the augmentation process that the vortex generators added to form the proposed design also conduct heat and add to the overall heat transfer surface. This influences the conductive process and affects the conductive flux. As demonstrated in the heat contour figure, figure 14. One notices that the vortex generators parallel to the pipes are of a red shade which indicates heat. This extra area of heat will allow the air flowing against it to convect more heat away from the condenser. It should be noted that in the manufacturing process of the proposed design, a good contact between the vortex generators and the fins needs to be created for this analysis to be useful.

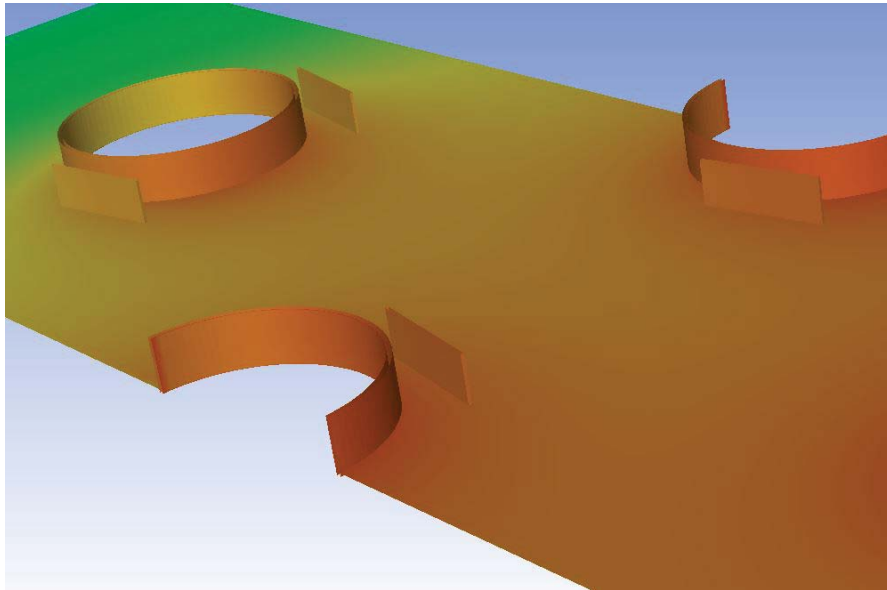


Figure 14: Conduction through pipe and fins.

Qualitative Analysis

The chief mechanism of cooling in the process of a heat transfer condenser is forced convection, which requires external power. The cost of the external power required has to be considered in the analysis and evaluation of an air-side cooling design. The amount of augmentation achieved by a condenser design is usually off set by the amount of power required to operate it and if the power costs outweigh the augmentation gains the design is not considered an improvement in a comparative study as one could simply run the original design at greater power. This has led to the invention of several qualitative analysis which have been proposed in order to distinguish between good and better designs, weighing the pressure drop and power requirements against the augmentation and heat transfer. Two commonly used non-dimensional number for this purpose are;

The **Skin Friction Coefficient / Fanning Friction Factor**, which is the ratio of wall shear stress to the reference dynamic pressure. It is described mathematically as;

$$f = C_f = \frac{\tau_w}{\frac{1}{2}\rho_{ref}v_{ref}^2} \quad \text{Where, } \rho_{ref}, v_{ref} = \text{reference density, reference velocity}$$
$$\tau_w = \text{wall shear stress}$$

The Fanning friction factor is useful as a qualitative assessment of the increase in friction and cost of operation. A second commonly used non-dimensional number usually calculated along side the Fanning friction coefficient is the **Colburn j-factor**, which yields a depiction of the augmentation achieved and is described as;

$$j = \frac{Nu}{RePr^{1/3}} = \frac{h}{\rho C_p V} Pr^{2/3} = StPr^{2/3}$$

where, St = the Stanton number

$$St = \frac{Nu}{RePr} = \frac{hD/k}{(D\bar{v}/\nu)(\nu/\alpha)} = \frac{h}{\rho C_p \bar{v}} = \frac{\text{Heat flux to the wall}}{\text{Convected heat flux}}$$

[25] The Colburn-j factor is useful for its qualitative assessment of the heat transfer augmentation.

In figure 15 we plot the Colburn-j factor from the area-weighted average surface Stanton number provided by Fluent. In each case we used the entrance velocity as the reference velocity for the calculation. We plot the Colburn j-factors for each simulation against their respective Reynolds numbers, utilising the hydraulic diameter defined as $4\frac{A_c}{A_t}L$ in Chapter 3. Many authors use different definitions for their hydraulic diameter, such as that for flow around a tube. We decided on this form of hydraulic diameter due to the complexity of the proposed design. The classic models and proposed models are plotted on the same graph for comparative reasons; As we expected the

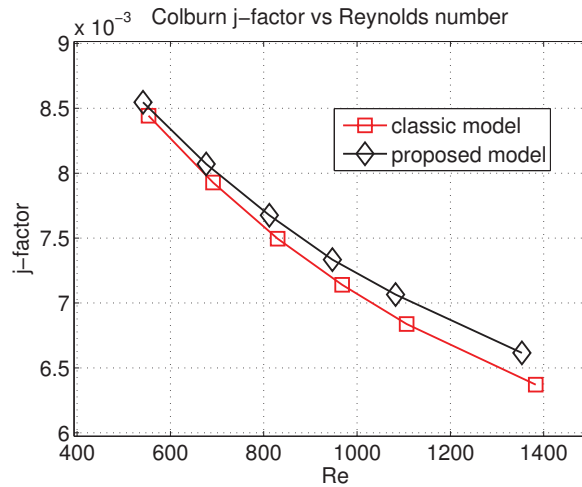


Figure 15: j-factor to Reynolds number

Colburn j-factor for the proposed design is higher than of the classic model, with the difference increasing as the Reynolds number increases. This qualitatively tells us that the proposed model has a better augmentation than the classic model. But at what cost?

The Fanning friction factor is plotted against the Reynolds number in figure 16, with the classic model and proposed model on the same graph. Here it is evident that the higher the Reynolds number the higher the cost of running the condenser and qualitatively for the same Reynolds number it is more expensive to run the proposed model than the classic model.

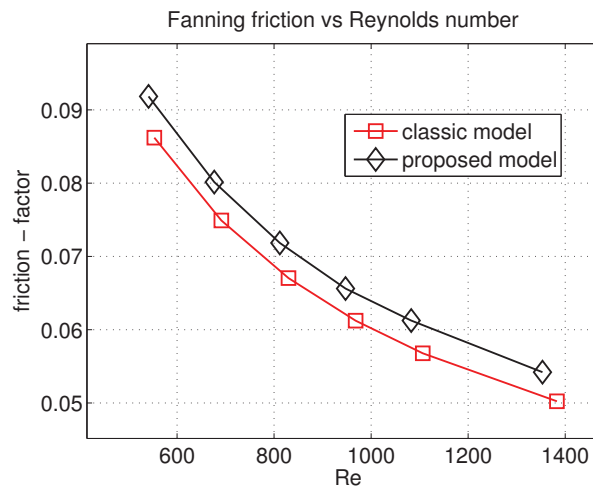


Figure 16: j-factor to Reynolds number

To assess the efficiency of the proposed model, given that there is a pressure penalty as well as an augmentation advantage. We describe several popular analysis that are used to quantify the advantage to penalty ratio. A popular analysis often used is known as the ‘area goodness’, described as $\frac{j}{f}$ and plotted against the Reynolds number [12]. The ‘area goodness’ analysis can be shown to be inversely proportional to the frontal flow area, which leads to the conclusion that a

higher area goodness factor will result in a device requiring a smaller frontal flow area resulting in a more compact device.

$$\frac{j}{f} = \frac{NuPr^{-1/3}}{fRe} \propto \frac{1}{A_e^2} \left(\frac{\dot{m}}{\Delta p} \right) \quad \text{where, } A_e = \text{ the entrance area,}$$

$$\dot{m} = \text{ mass flow rate, } \Delta p = \text{ pressure drop}$$

This analysis has however been described as “not infallible” and for comparative purposes requires a fixed, mass flow to pressure drop ratio, $\left(\frac{\dot{m}}{\Delta p} \right) = \text{constant}$ [21]. The “area goodness” analogy can also be misleading as a compact heat exchanger with an enhancement element is typically characterised by an increase in pressure drop. The increase in pressure drop leads to an increase in the Fanning friction factor f , which is usually larger in percentage than the increase in Nusselt number, and therefore j -factor. This can lead to incorrect conclusions that less compact heat exchangers are more efficient [16].

Another prominent ‘goodness factor’ suggested by Kays and London, [12] [21] which is more relevant to our work is the ‘volume goodness factor’ which compares the average surface heat transfer coefficient, and a power formulation, which they define as;

$$h = \frac{kNu}{D_h} \quad \text{where } Nu = \text{ Nusselt number , } k = \text{ thermal conductivity coefficient}$$

$$D_h = \text{ hydrostatic diameter , } \dot{m} = \text{ mass flow rate}$$

$$E = \frac{\dot{m}\Delta p}{\rho A_t} = \frac{A_c}{A_t} \vec{v} \Delta p \quad A_c = \text{ entrance area , } A_t = \text{ heat transfer area}$$

$$\vec{v} = \text{ entrance velocity , } \Delta p = \text{ pressure drop}$$

[21] and more recently an alternative ‘volume goodness factor’ is being suggested in the literature

as describing a quantification of good heat transfer and pressure loss performance. It is being calculated as; $\frac{j}{f^{1/3}}$ and plotted against the Reynolds number [6] [17] [4]. This analogy has also led to a ‘thermohydraulic performance factor’, which is calculated as;

$$JF = \frac{j/j_c}{(f/f_c)^{1/3}} \quad \text{where, } j_c = \text{j-factor of the reference or classic model}$$

$$f_c = \text{friction factor of reference or classic model}$$

[6] [4]

In figure 17 we plot the ‘volume goodness’ factor as described by Kays and London, for both the classic models and proposed models such that we can make a comparison.

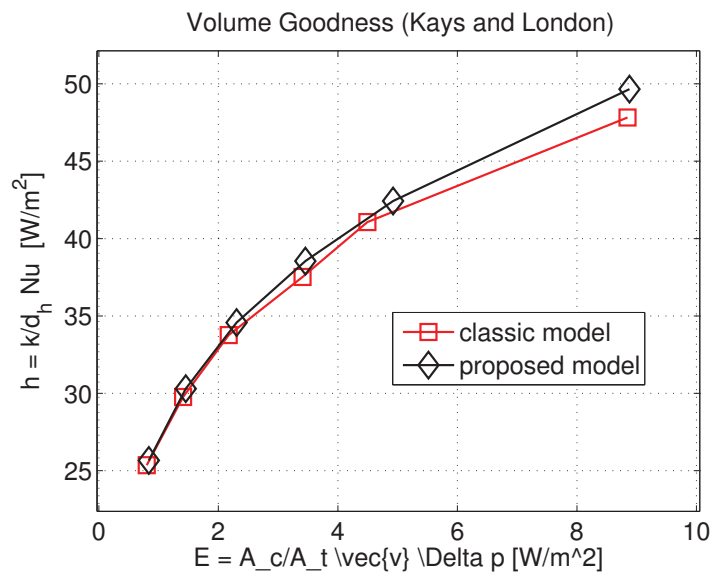


Figure 17: Volume Goodness (Kays and London 1984)

Form the comparison plot of figure 17, it can be seen that at low Reynolds numbers there ap-

pears to be no advantage to using the proposed model. Although the analysis does not suggest a disadvantage to the proposed model. An advantage of the proposed model becomes evident as the Reynolds numbers increase, with a more pronounced advantage at face velocity values of 3.5 m/s and 5.0 m/s, which are the limits of the suggested operating face velocities by, Capitol Coil & Air, who recommend 800 ft/min \approx 4.0 m/s as optimal [1].

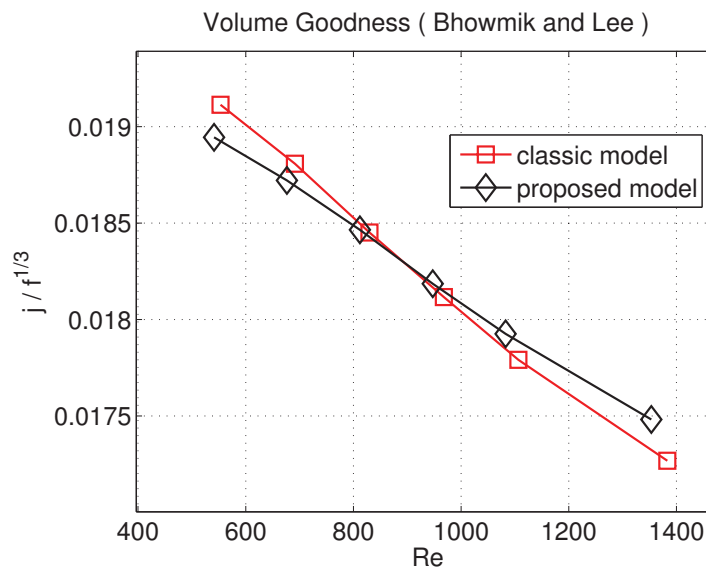


Figure 18: Volume Goodness (Bhowmik and Lee 2008)

In figure 18 we plot the more recent ‘volume goodness’ analogy suggested by Bhowmik and Lee. We plot the classic models next to the proposed models for a comparison.

The plots in figure 18 suggest there is a disadvantage to the proposed model at lower Reynolds numbers and that this becomes an advantage above face velocities above 3.5 m/s. The figure also suggests greater improvement with greater Reynolds numbers.

In figure 19 we plot the ‘thermohydraulic performance’ as suggested by Bhowmik and Lee [4] [6]. The figure suggests a positive advantage for using the proposed model at face velocities above 3.0 m/s and a penalty for use of the proposed model at velocities below 3.0 m/s. The figure; 19 also suggest an increase in efficiency as the face velocities increase.

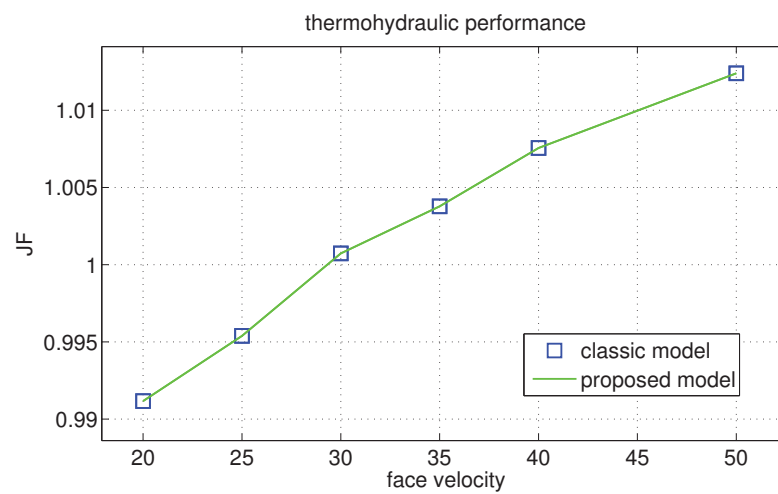


Figure 19: thermohydraulic performance factor

Criticism of the ‘volume goodness factor’ comes from its dependence on the hydraulic diameter of the system. To try and overcome some of this criticism of the ‘volume goodness factor’, a set of dimensionless ‘performance parameters’ were proposed by LaHaye et al [21]. They are the heat transfer ‘performance factor’, $J = jRe_h$ which is plotted against the ‘pumping power factor’, $P = fRe_h^3$. There has been criticism of the ‘performance parameter’ which stems from its dependence on the Reynolds number which can be difficult to define in an altered flow channel. It is therefore seen as only a useful approximation to direct a designer in the vicinity of an optimal

solution [21]. This then led Soland et al [19] to modify the ‘performance factors’ further. As knowledge of the heat transfer rate and area is known and given the relationship with the number of transfer units (NTU) $hA_T = \frac{q}{\Delta T} \propto NTU$ where, A_T = heat transfer area. The number of transfer units (NTU) is a very significant factor in a heat exchanger, as it quantifies how much heat is leaving the system. We can thus qualitatively plot the NTU against the ideal power required calculated as, $\Delta P|\vec{v}|A_e$ where, A_e = flow entrance area. As this information is available through a CFD simulation with Fluent 18, a very informative comparison can be made 20. $|\vec{v}|$ = the magnitude of air flow velocity at the entrance[21].

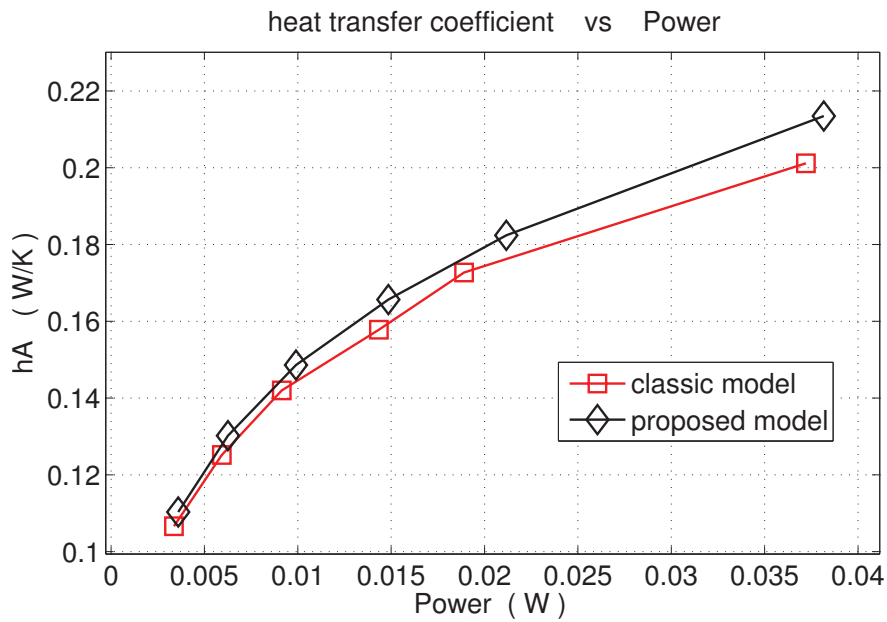


Figure 20: Number of Thermal Units to Power Plot.

Although similarly composed to the Kays and London formulation of the ‘volume goodness’, this analysis shows more clearly the amount of heat being removed compared with the amount of

ideal power required. In the figure 20 there is a clear separation between the proposed models plotted and the classical models.

It is an advantage of CFD modelling in that we can calculate numbers for quantities that are much harder to analyse via experimental work. Although, empirical results do account for certain quantities that go unaccounted for in an idealised CFD simulation like this study. We can also quantify and calculate the heat flux to both ideal power and Reynolds number, as we do in figures 22 and 21 respectively.

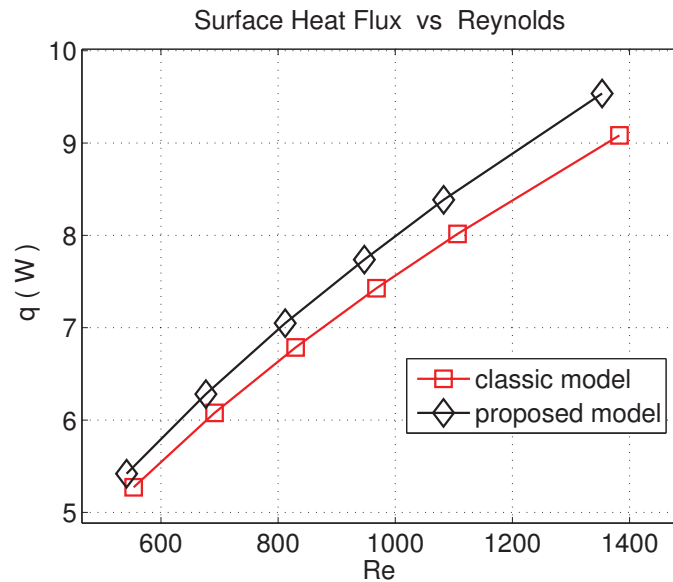


Figure 21: The heat flux as a function of Reynolds number

In figure 21 we plot the classic models and proposed models heat transfer flux to Reynolds number which shows the heat flux of the proposed model continuously higher than the classic model over all Reynolds numbers, with the difference increasing with Reynolds number. In figure 22 we plot the heat transfer flux as a function of the ideal power for both models as a comparison.

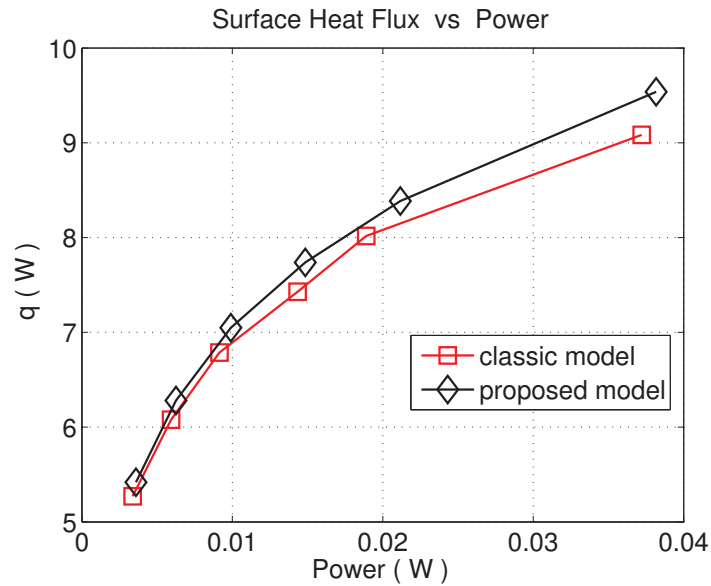


Figure 22: The heat flux as a function of Power

The outcome of the figure 22 is much the same as figure 20. It demonstrates an almost logarithmic shape to the functions of both the classic models and proposed models, suggesting that the gain in heat flux tappers with the increase in power. The figure also suggests that the proposed model will consistently generate a higher heat flux over the system than a classic flat-plate fin and pipe design.

Criticism of Design

It should be mentioned that a potential consequence of the proposed design, is an increased potential for the trapping of foreign objects between the vortex generators and the pipes. As the spacing between the vortex generators and pipes is smaller than that of the channel entrance, objects may enter the channel becoming trapped between the vortex generators and pipes, remaining there unnoticed and undetected. If this were to happen, it would create a considerable hinderance

to the heat transfer process and we predict it could lead to an inefficient airside condenser design.

Interpretation

Seeking to quantify the improvement that can be stated for our proposed design, we view the data in terms of percentage gains and percentage costs. In figure 23 we lay out the ideal power, surface heat transfer coefficient \times area ha and heat flux q for each of the simulations we ran. We then make a percentage comparison of those functions between the proposed model and the classic model at each face velocity we simulated.

Model	Velocity	Power [W]	ha [W/K]	q [W]	% ha gain	% q gain	% Power cost
Classic	2.0 [m/s]	0.0034	0.1066	5.2711			
Proposed	2.0 [m/s]	0.0036	0.1103	5.4182	3.448 %	2.790 %	6.648 %
Classic	2.5 [m/s]	0.0059	0.1252	6.0774			
Proposed	2.5 [m/s]	0.0063	0.1302	6.2803	4.0324 %	3.337 %	5.51 %
Classic	3.0 [m/s]	0.0091	0.1420	6.7863			
Proposed	3.0 [m/s]	0.0099	0.1486	7.0491	4.6507 %	3.873%	8.339 %
Classic	3.5 [m/s]	0.0143	0.1578	7.4284			
Proposed	3.5 [m/s]	0.0149	0.1657	7.7370	4.9664%	4.154 %	3.545 %
Classic	4.0 [m/s]	0.0189	0.1727	8.0164			
Proposed	4.0 [m/s]	0.0212	0.1824	8.3859	5.596 %	4.609 %	11.965 %
Classic	5.0 [m/s]	0.0372	0.2012	9.0838			
Proposed	5.0 [m/s]	0.0382	0.2135	9.5371	6.1138 %	4.990%	2.571%

Figure 23: Chart of percentage gains and losses

We find that figure; 23 demonstrates that the power, surface heat transfer coefficient ha and heat flux monotonically increase with an increase in the velocity. The percentage gains found in the surface heat transfer coefficient ' ha ' as well as the heat flux ' q ', in simulations using the proposed model also monotonically increase with the air face velocity. However, the percentage power cost

in simulations using the proposed model fluctuates with the various air face velocity simulations. The greatest % increase in power costs for using the proposed model in our simulations is found at 4.0 m/s air face velocity, which is the recommended optimum operational condition proposed by Capitol Coil & Air [1], with the lowest power cost in our simulations found at the edges of the recommended face velocities. From this perspective it can be suggested that running the condenser at air face velocities of 5.0 m/s, where the highest percentage gains are and the lowest percentage power costs are would be the most advantageous operating conditions.

In terms of modifying a heat transfer device to add a saving in power output, one would then seek to run the device at the same heat transfer rate or heat flux. As our simulations have not been constructed for such a comparison we can only make an approximation by using a linear interpolation of the proposed models power at the maximum heat transfer rate of the classical model running at the recommended face velocity of 4.0 m/s. We also make comparison at the heat transfer rate of the classic model running at 5.0 m/s.

We find the resultant percentage saved at 4.0 m/s comparison to be; 7.06 % and the power saved at 5.0 m/s is ; 15.42 %.

Although it should be noted that the power is considered ideal and calculated as, $\vec{v}A_c\Delta p$. A real pressure drop device, would have an efficiency factor that would scale with the air face velocity it produces. The energy saving is also calculated over a very small incident of the total heat transfer device and as the temperature difference between the inlet air temperature and pipe water temperature decrease, the potential for energy saving might be significantly affected.

CHAPTER 7

CONCLUSIONS

Fluent's finite volume solver enabled us to numerically solve the most relevant equations in order to conduct a comparative study on a new design of an airside condenser utilising vortex generators to disrupt the flow. We found that the flow is disrupted in such a way as to transport some of the stagnant heated air that collects in the wake of the condenser pipes. From our analysis of the results of comparisons over 6 varying face velocities, we can conclude that there is evidence that our design will improve the heat augmentation and or save energy. We predict that the energy saved could be reach upward of 15%.

Future research

Future work on the subject could include a comparison of models, varying the angle of the vortex generators, varying the distance of the vortex generators from the pipe and deviating slightly from the theme of cost effective construction or alteration, a simulation of vortex generators with a foil design could yield very positive results. Of course empirical data would be best and once a preferable angle and position has been decided, a small condenser could be altered with the vortex generators and experimental data would be conclusive.

BIBLIOGRAPHY

- [1] C. C. . Air. Fluent theory guide 6.1, 2018.
- [2] J. D. Anderson. *Fundamentals of Aerodynamics*. McGraw-Hill 1221 Avenue of the Americas, New York, NY 10020, 3rd edition.
- [3] F. Ansys. *Fluent User Guide 13*. ANSYS, Inc., 13 edition.
- [4] H. K.-S. L. Bhowmik. Analysis of heat transfer and pressure drop characteristics in an offset strip fin heat exchanger. *International Communications in Heat and Mass Transfer*, 36:259–263, 2009.
- [5] C.-C. W. K.-Y. Chi. Heat transfer and friction characteristics of plain fin-and-tube heat exchangers, part i: new experimental data. *International Journal of Heat and Mass Transfer*, 43:2681 – 2691, 2000.
- [6] M. D. B. Erbay, B. L. Ozturk. *Comprehensive Study of Compact Heat Exchangers with Offset Strip Fin, Heat Exchangers - Advanced Features and Applications S. M. Sohel Murshed*. IntechOpen, DOI: 10.5772/66749., chapter 3 edition.
- [7] T. H. R. Eymard, R. Gallouet. *Finite Volume Methods: Update to Handbook of Numerical Analysis*. P.G. Ciarlet, J.L. Lions eds, 7 edition.
- [8] M. S. E. A. J. Gorman, J.M. Carideo. Heat transfer and pressure drop comparison of louver-and plain-finned heat exchangers where one fluid passes through flattened tubes. *Case Studies in Thermal Engineering*, 5:122–126, 2015.
- [9] D. M. J. J. J. Hwang, S.W. Kim. Cfd analysis of fin tube heat exchanger with a pair of delta winglet vortex generators. *Journal of Mechanical Science and Technology*, 26:2949–2958, 2012.
- [10] F. inc. Fluent theory guide 6.1, 2006.
- [11] L. M. Jiji. *Heat Convection*. Springer-Verlag, Berlin Heidelberg, 2nd edition.
- [12] A. Kays, W.M. London. *Compact Heat Exchangers*. McGraw Hill, New York, 3rd edition.
- [13] F. Menter. Two-equation eddy-viscosity turbulence models for engineering applications. *AIAA Journal*, 32,No.8:1598–1605, 1994.
- [14] T. H. H. W. R. A. P. Munson, B.R. Okiishi. *Fluid Mechanics*. John Wiley & Sons Singapore Pte. Ltd., 7th edition.
- [15] E. N. L. R. Byron Bird, Warren E. Stewart. *Transport Phenomena*. John Wiley & Sons, Inc., 2nd edition.

- [16] F. D. A. Sahiti, N. Durst. Strategy for selection of elements for heat transfer enhancement. *International Journal of Heat and Mass Transfer*, 49:3392–3400, 2006.
- [17] K. S. Shobhana Singh. Numerical investigation of conjugate heat transfer and flow performance of a fin and tube heat exchanger with vortex generators. *Proceedings of the 58th Conference on Simulation and Modelling (SIMS 58) Reykjavik, Iceland.*, 138:13–19, 2017.
- [18] D. R. S. H. J.-L. Simo Tala, J.V. Bougeard. Tube pattern effect on thermalhydraulic characteristics in a two-rows finned-tube heat exchanger. *International Journal of Thermal Sciences*, 60:225–235, 2012.
- [19] W. R. W. Soland, G.J. Mack Jr. Performance ranking of plate-fin heat exchanger surfaces. *Trans. ASME J. Heat Transfer*, 100:514–519, 1978.
- [20] J. L. Z. Song, W.M. Meng. Numerical study of air-side performance of a finned flat tube heat exchanger with crossed discrete double inclined ribs. *Applied Thermal Engineering*, 30:1797–1804, 2010.
- [21] K. Stone. Review of literature on heat transfer enhancement in compact heat exchangers. *Air Conditioning and Refrigeration Center Technical Reports*, 1996.
- [22] J.-C. J. Tzong-Shing Lee, Wu-Chieh Wu. Improved energy performance of air-cooled water chillers with innovative condenser coil configurations- part ii: Experimental validation. *International Journal of Refrigeration*, 35:2212–2222, 2012.
- [23] J. L. Y. W.-C. Wang, C. Lo. Flow visualization of annular and delta winlet vortex generators in fin-and-tube heat exchanger application. *International Journal of Heat and Mass Transfer*, 45:3803–3815, 2002.
- [24] K.-Y. L.-J. T.-C.-Y. Wang, C-C. Chen. An experimental study of the air-side performance of fin-and-tube heat exchangers having plain, louver, and semi-dimple vortex generator configuration. *International Journal of Heat and Mass Transfer*, 80:281–287, 2015.
- [25] P.-J. S. Wei-Mon Yan. Heat transfer and friction characteristics of fin-and-tube heat exchangers. *International Journal of Heat and Mass Transfer*, 43:1651–1659, 2000.

CURRICULUM VITAE

David Vallet

Department of Mechanical Engineering
University of Nevada, Las Vegas
Las Vegas, Nevada
NV 89154, USA

vallet@unlv.nevada.edu

EDUCATION

ACADEMIC

University of Nevada Las Vegas, U.S.A
M.S. Mechanical Engineering August 2016 - Present

University of South Africa, Pretoria, R.S.A
B.Sc. honours., Applied Mathematics, June 2017
B.Sc., Mathematics and Applied Mathematics, June 2015

Crawford College, Johannesburg, R.S.A
Matric Certification (High School), December 1993

EDUCATION

OTHER

South African Tourist Guide qualifications, June 2013
TG23 Rock Climbing
TG25 Mountain Walking
TG26 Mountaineering

American Mountain Guide qualifications
AMGA certified Alpine Guide, 2009
AMGA certified Rock Guide, 2007

Tirolean Ski Instructor qualifications
Landesschilehrerprüfung, 2001
Schilehrer - Anwarterprüfung, 2000
